



# Electrodes and Electric Field Distribution in Clinical Practice

Helena Cindrič , Bor Kos , and Damijan Miklavčič 

## Abstract

The success of electroporation-based treatments (i.e., reversible electroporation for electrochemotherapy and gene electrotransfer and irreversible electroporation as a tissue ablation method) depends on complete coverage of the clinical target volume with a sufficiently strong electric field (exceeding the reversible or irreversible electroporation threshold, depending on the type of treatment). Electric field distribution in biological tissue is a complex phenomenon that depends on several parameters, such as the electrode geometry, parameters of delivered pulses and tissue composition and electrical properties. Numerical modelling has proven to be an indispensable tool in investigating and designing electroporation-based treatments and preparing patient-specific treatment plans. In this chapter, the basic principles regarding electric field distribution in biological tissue are explained, with the aim to enable effective electroporation-based treatments. Biological effects observed in electroporation on tissue level are described, common electrode designs used in clinical practice are shown and equipped also with simple models of electric field distribution. The basic principles of numerical modeling and treatment planning are also explained.

## Keywords

Electric field distribution · Electrodes for electroporation · Numerical models · Treatment planning · Clinical practice · Tissue electroporation

H. Cindrič · B. Kos · D. Miklavčič (✉)

Faculty of Electrical Engineering, University of Ljubljana, Ljubljana, Slovenia

e-mail: [helena.cindric@fe.uni-lj.si](mailto:helena.cindric@fe.uni-lj.si); [bor.kos@fe.uni-lj.si](mailto:bor.kos@fe.uni-lj.si); [Damijan.miklavcic@fe.uni-lj.si](mailto:Damijan.miklavcic@fe.uni-lj.si)

© The Author(s), under exclusive license to Springer Nature Switzerland AG 2021

J. A. Impellizeri (ed.), *Electroporation in Veterinary Oncology Practice*,

[https://doi.org/10.1007/978-3-030-80668-2\\_2](https://doi.org/10.1007/978-3-030-80668-2_2)

# 1 Introduction

Electroporation is a phenomenon in which short high-voltage electric pulses are used to change the structural integrity of the cell membrane and consequently increase the membrane permeability. With an appropriate selection of pulse parameters—namely the amplitude, duration, and number of applied pulses—the phenomenon can be either reversible or irreversible. In reversible electroporation, the cell membranes quickly return to their original state and the cells' ability to divide and function is not affected in the long term, while in irreversible electroporation the cells lose their functionality due to high exposure and die (Neumann and Rosenheck 1972; Kotnik et al. 2011, 2019; Rems and Miklavčič 2016). Electroporation has sparked interest for use in medicine, biotechnology, and food processing (Yarmush et al. 2014; Mahnič-Kalamiza et al. 2014; Kotnik et al. 2015; Geboers et al. 2020). In medical applications reversible electroporation is used for facilitating the transport of various molecules into cells, the most promising treatments being electrochemotherapy (ECT) and gene electrotransfer (GET) (Mir et al. 1991; Serša and Miklavčič 2008; Rosazza et al. 2016; Stepišnik et al. 2016), while irreversible electroporation (IRE) is used for ablation of tumor and cardiac tissue (Davalos et al. 2005; Edd et al. 2006; Rubinsky 2007; Meijerink et al. 2018; Jiang et al. 2015; Scheffer et al. 2014; Reddy et al. 2018; Wittkampf et al. 2018; Stewart et al. 2019).

It is generally accepted that reversible and irreversible electroporation occurs in tissue at a specific electric field strength, i.e., the reversible and irreversible electroporation threshold (Fig. 1). A complete coverage of the target tissue volume with electric field above either the reversible or the irreversible threshold is required to achieve a therapeutic effect in electroporation-based treatments (Miklavčič et al.

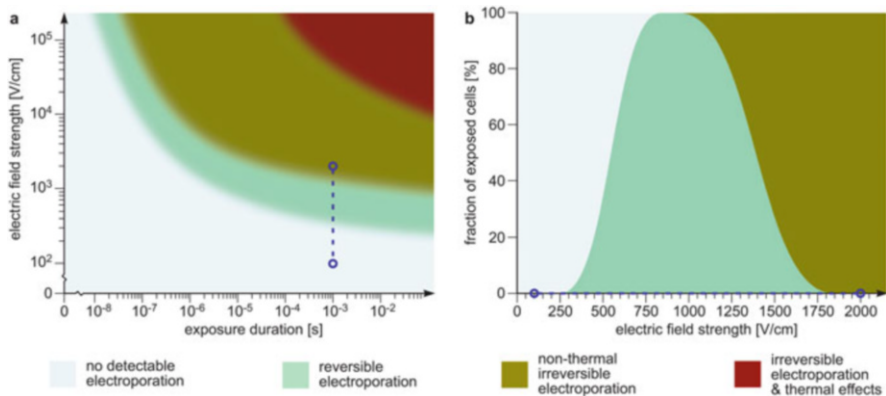


**Fig. 1** (a) Reversible and irreversible electroporation and thermal effects are functions of both the electric field strength and the duration of tissue exposure (mainly the number and duration of applied pulses). Electroporation may occur at lower electric field threshold if exposure duration is increased. (b) For a fixed exposure duration of 1 ms (dashed line in panel a), the fraction of electroporated cells is a function of the electric field strength. The image is reproduced from Yarmush et al. (2014)

2006). Electric field distribution in tissue depends on the electrode geometry, parameters of delivered pulses, and tissue electrical properties. Several electrode designs and configurations have been developed through the years to support different therapeutic needs—from plate electrodes mainly used for the treatment of superficial tumors (e.g., skin metastases), fixed needle arrays, individual needle electrodes for treatment of deep-seated tumors, to electrodes tailored to specific treatments such as finger electrodes (Miklavčič et al. 2014; Geboers et al. 2020). The geometry of the electrodes largely determines the distribution of electric fields in tissue.

A wide range of different pulses and pulse protocols is used in practice—from  $8 \times 100\mu\text{s}$  pulses used in ECT to  $90 \times 100\mu\text{s}$  pulses used in IRE, and millisecond pulses used in GET. The most straightforward approach to controlling the electric field strength is by adjusting the applied voltage amplitude according to the distance between paired electrodes. The manufacturers of pulse generators usually suggest a fixed voltage-to-distance ratio as the guideline for applied voltage amplitude. However, voltage-to-distance ratio should not be confused with the electroporation thresholds (despite sharing the same unit of measure—V/cm), as it is generally higher than the actual threshold. Electroporation thresholds also depend on the duration of exposure of target tissue to the electric field, i.e., the number and duration of applied pulses (Pucihar et al. 2011). In other words, electroporation may occur at a lower threshold if more pulses or longer pulses are applied, as demonstrated in Fig. 1.

Another important factor affecting the electric field distribution is tissue properties. Target tissue is often not a homogenous structure and may include different tissue types (e.g., skin, fat, and muscle in case of treatment of cutaneous and subcutaneous targets), which have different electrical and thermal properties. The local electric field strength depends on the electrical conductivity of the medium (i.e., tissue), therefore, any inhomogeneity in tissue electrical conductivity affects the electric field distribution, and needs to be accounted for when planning the treatment (Dermol-Černe et al. 2020). Furthermore, tissue electrical conductivity is not constant during electroporation but increases due to electroporation, which depends on the local electric field strength in the tissue, and due to increased temperature. This rise in electrical conductivity in turn affects the local electric field (Šel et al. 2005; Ivorra et al. 2009; Corovic et al. 2013).

Electric field distribution in biological tissue is a complex phenomenon with multiple factors to be considered and is, therefore, often not intuitive or easy to determine. This chapter provides an overview of basic principles regarding electric field distribution in biological tissue, with the aim to enable effective electroporation-based treatments (i.e., reversible electroporation for electrochemotherapy and gene electrotransfer and irreversible electroporation as a tissue ablation method). Biological effects of electroporation on tissue level are explained and common electrode designs for clinical practice are shown and equipped with results based on contemporary numerical models. The basics of numerical modelling and patient-specific treatment planning are also provided.

## 2 Gross Biological Effects Observed in Electroporation

### 2.1 Reversible Electroporation

When a biological cell is exposed to an external electric field of sufficient strength structural and chemical changes occur primarily in the cell membrane but also in other subcellular structures, such as the cytoskeleton. This process is known as electroporation or electropermeabilization. So far, three main mechanisms affecting the cell membrane have been identified (Kotnik et al. 2019): (a) the formation of hydrophilic pores in the lipid bilayer, (b) chemical changes in membrane lipids (e.g., peroxidation), and (c) electrically induced modulation of membrane protein function (e.g., voltage-gated channels). These mechanisms contribute to a transiently increased permeability of the cell membrane to water, ions, and molecules of various sizes, for which the membrane is otherwise impermeable or poorly permeable. The membrane gradually recovers its physiological level of impermeability (resealing) within a few minutes after the termination of pulse delivery and, unless the damage inflicted is leading to cell death, the membrane returns to its natural state within a few hours. Electroporation causes the formation of additional conductive pathways in the otherwise poorly conducting cell membrane thus also resulting in an increased bulk electrical conductivity of affected tissue. Figure 2 shows a diagram of various gross biological effects encountered in electroporation treatments. The zone of reversible electroporation is indicated in Fig. 2 with a yellow contour.

Facilitation of cellular uptake by reversible electroporation is the basis of electrochemotherapy (ECT) and gene electrotransfer (GET), in which cytotoxic agents and genetic material, respectively, are introduced into cells. The membrane resealing mechanism traps the introduced material within the cell thus increasing its effectiveness. ECT has already achieved a firm place in clinical and veterinary oncology (Cemazar et al. 2008; Kulbacka et al. 2017; Campana et al. 2019) with the introduction of the European Standard Operating Procedures of ECT (ESOPE) in 2006 (Mir et al. 2006; Gehl et al. 2018). GET is not yet in widespread use in humans, but ongoing studies show promising results. Currently, the most advanced applications of GET are DNA vaccination and cytokine therapy (Heller and Heller 2015; Lambrecht et al. 2016; Geboers et al. 2020).

### 2.2 Irreversible Electroporation

If the applied electric field exceeds a critical threshold, the cell membrane is damaged to the extent that it can no longer repair itself, resulting in loss of cell homeostasis. The damaged cells eventually die in a mechanism that is similar to the programmed cell death known as apoptosis (Yarmush et al. 2014; Rems and Miklavčič 2016). This process is known as irreversible electroporation and has attracted interest as an alternative method for ablation of various soft tissues due to its essentially nonthermal cell kill mechanism (Davalos et al. 2005; Scheffer et al. 2014; Aycock and Davalos 2019).

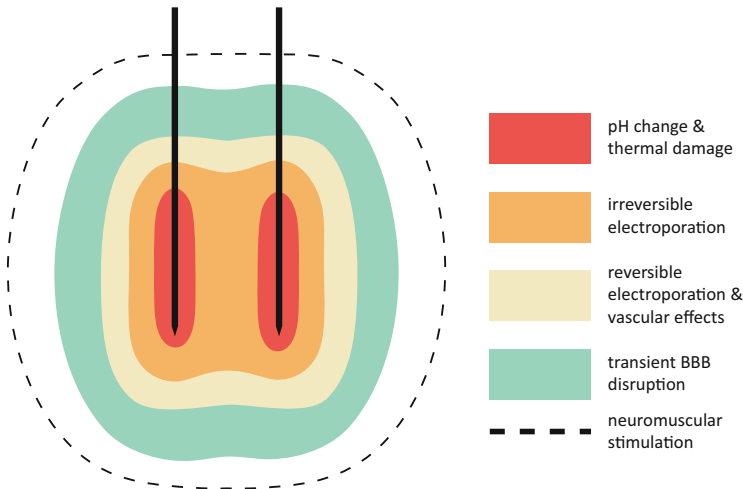


**Fig. 2** Regions of gross biological effects observed in electroporation. Mechanical damage occurs along the path of needle electrode insertion. Thermal damage and possible pH changes occur in close proximity to the electrode surface (red), followed by a zone of irreversible electroporation (orange), a zone of reversible electroporation and vascular effects (yellow), and a zone of transient blood–brain barrier (BBB) disruption (green). The dashed contour indicates the zone where excitable tissues, such as nerves and muscles, are stimulated. It should be noted that this diagram is for illustrative purposes only. The size of specific regions varies with many parameters, including electrode spacing and length of exposed tip, duration and number of applied pulses, and tissue type. Moreover, the specific effects do not necessarily overlap with reversible/irreversible electroporation, for instance vascular effects may manifest already at lower electric fields than reversible electroporation

In the therapeutic setting, several cell death mechanisms are likely to act in addition to apoptosis, including necrosis caused by the inevitable thermal component (Ben-David et al. 2012; Garcia et al. 2014), necroptosis, and the contribution of the systemic immune response targeting the tumor and potential metastatic sites (Brock et al. 2020). Irreversible electroporation affects mainly the cells, leaving other structures and proteins in the extracellular matrix intact, thus maintaining the structural integrity of the tissue. This promotes tissue regeneration after treatment and reduces tissue scarring, which is a significant improvement compared to existing treatment modalities (Vogel et al. 2016). The zone of irreversible electroporation is indicated in Fig. 2 with an orange contour.

Even though lower pulse amplitudes and significantly fewer pulses are used in electrochemotherapy, an area of irreversibly electroporated tissue is also present. However, this area is limited to a few millimeters from the electrode surface and has little clinical significance for ECT (Zmuc et al. 2019). Similarly, a zone of IRE is also to be expected in GET, as longer pulses are used. In GET reversible electroporation and cell survival are imperative for successful transfection, therefore, irreversible electroporation is undesirable (Lacković et al. 2009). Moreover, the associated

heating and pH changers may also negatively affect the plasmid DNA (Maglietti et al. 2013).

### 2.3 Thermal Effects

Electroporation, and especially IRE ablation, is commonly referred to as a nonthermal modality, which can lead to a wrongful assumption that the thermal component is completely absent from the treatment. No clinically relevant heating has been observed in treatments with reversible electroporation. However, in IRE ablation, several studies have shown that current clinical protocols may lead to elevated temperatures sufficient to cause thermal damage to varying degrees (Ben-David et al. 2012; Faroja et al. 2013; Dunki-Jacobs et al. 2014; Wagstaff et al. 2015). When an electric current flows through a conducting medium, thermal energy is generated in a process called Joule heating. High voltages (up to 3000 V) are used in IRE ablation and several hundred pulses are sequentially delivered in a single session, especially when treating large volumes of tissue with multiple electrode pairs. While the predominant cell death mechanism in IRE is still nonthermal, these factors do contribute to a distinct thermal component that results in an area of necrotic tissue consistent with thermal injury. The area of thermal damage is mostly confined to the vicinity of the electrodes and may extend further into the surrounding tissue as the number and duration of pulses increases (Garcia et al. 2011; O'Brien et al. 2018). The zone where thermal damage is expected is indicated in Fig. 2 with a red contour.

The currently most common application of IRE ablation is in treatment of tissue volumes where the use of conventional treatments, such as surgery, radiofrequency ablation, and microwave ablation, are contraindicated for various reasons. Due to its predominantly non-thermal mechanism of cell kill, IRE ablation has shown promise for use in cases where other ablation modalities present an unacceptable risk to nearby critical anatomical structures such as vessels, bile ducts, and nerve bundles that are highly susceptible to thermal damage (Maor et al. 2010; Schoellnast et al. 2013; Cannon et al. 2013). However, in such cases, the thermal component of IRE ablation cannot be neglected. Special care must be taken to place the electrodes at a sufficient distance from the critical anatomical structures and pulsing protocols used during treatment must be carefully considered. Recent studies have demonstrated the potential of internally cooled electrodes (O'Brien et al. 2018) and algorithmically controlled pulsing protocols (Sano et al. 2020) for regulating the temperature during ablation. In addition, IRE is unaffected by the heat sink effect and can, therefore, be successfully used for ablation in the vicinity of large blood vessels, where the efficacy of thermal ablation modalities is reduced (Ahmed et al. 2011).

## 2.4 Blood Flow Modifying Effects of Pulsed Electric Fields

It is well known that electroporation induces a decrease in local blood flow, which may be roughly divided into two phases. Immediately after the initiation of pulse delivery the local blood flow reduces nearly to zero within a few seconds. This rapid decrease is mainly attributed to the constriction of smooth muscles in the vessel walls (vasoconstriction). This phase is relatively short, as blood flow recovers to about 40% of pre-treatment levels in up to 15 min after pulse application (Jarm et al. 2010). After the initial recovery, a stall in blood flow recovery is observed in the second phase, mainly due to structural changes in the endothelium. Electroporation causes disruption of the cytoskeletal filaments and intercellular junctions resulting in increased permeability of the endothelial monolayer (Kanthou et al. 2006; Čemažar 2017). Loss of barrier integrity leads to fluid leakage, resulting in increased interstitial fluid pressure and decreased intravascular pressure (Jarm et al. 2010; Graybill and Davalos 2020). These factors together manifest in decreased local perfusion, which may persist for several hours after treatment. The decrease in perfusion is more pronounced in tumor tissue than in healthy tissue because of the already abnormal vasculature of tumors, and may persist for up to 24 h after treatment. The zone of vascular effects corresponds roughly with the zone of reversible electroporation and is indicated in Fig. 2 with a yellow contour.

The vascular effects of electroporation have further relevance in electroporation-based treatments. While the application of pulses alone causes a temporary decrease in blood flow, the addition of the chemotherapeutic agent in ECT has been shown to cause permanent disruption of local vasculature (Čemažar 2017). The vascular disrupting effect of ECT is already effectively used in the treatment of bleeding metastases (Jarm et al. 2010) and is also beneficial in the treatment of highly vascularized organs, such as the liver. Moreover, it prevents washout of cytostatic drugs in ECT and plasmids in GET. On the other hand, a reduction in tissue perfusion also leads to a decreased cooling ability of the affected tissue. In IRE ablation, a large number of pulses is applied to the target tissue; therefore, Joule heating by the electrodes is more pronounced and results in a greater thermal component. A decrease in tissue blood perfusion may contribute even further to the undesirable thermal component by reducing the amount of heat that the blood is able to extract from tissue.

## 2.5 Nerve and Muscle Stimulation

Excitable tissues, such as muscles, nerves, and myocardium, respond to external electrical stimuli, and the electric field threshold for triggering the action potential in excitable cells is much lower than that of electroporation. Therefore, the application of electroporation pulses causes stimulation of nerves and muscles in the vicinity of the treatment zone, resulting in muscle contractions and acute pain (Golberg and Rubinsky 2012; Mercadal et al. 2017). The zone of neuromuscular stimulation is indicated in Fig. 2 with a dashed contour.

Several advances have been made to reduce the neuromuscular stimulation during electroporation-based treatments. Local or general anesthesia (depending on treatment type) is used to reduce pain during pulse application, while muscle relaxants are used to reduce muscle contractions; however, contractions are still observed near the electrodes (Golberg and Rubinsky 2012). Aside from unpleasant sensations, muscle contractions can displace the electrodes during treatment. This is particularly important during IRE ablation of deep-seated tissues, where long needle electrodes are carefully placed around the target volume. Displacement of the electrodes during pulses alters the electric field distribution and increases needle trauma, which can lead to undertreatment and harmful effects on nearby vital structures (Martin et al. 2015). Therefore, in current clinical practice, all IRE procedures are performed under general anesthesia with complete neuromuscular blockade. Furthermore, to eliminate the risk of triggering cardiac arrhythmias during procedures in the thoracic region, synchronization of pulse delivery with the patient's ECG cycle is required; pulses are timed to be delivered during the absolute myocardial refractory period (Cannon et al. 2013; Mali et al. 2015).

Several studies have shown that altering pulse dynamics, for example, increasing the pulse repetition rate of monopolar pulses from 1/s to 5000/s in ECT (Miklavčič et al. 2005; Zupanic et al. 2007), can significantly reduce muscle stimulation and associated adverse effects without compromising treatment efficacy. A new pulse protocol for IRE, referred to as high-frequency IRE or H-FIRE has been introduced in recent studies (Arena et al. 2011; Yao et al. 2017; Ringel-Scaia et al. 2019), in which conventional monopolar pulses with a repetition rate of 1–5000/s are replaced by bursts of bipolar pulses with a repetition rate of 50,000–125,000/s.

## 2.6 Blood–Brain Barrier Disruption

The blood–brain barrier (BBB) is a multicellular endothelial structure that separates the central nervous system from the peripheral vasculature and restricts the passage of pathogens and various molecules from the blood into the cerebrospinal fluid (Obermeier et al. 2013). Due to its high selectivity, BBB is a major obstacle to the effective penetration of systemically administered therapeutics, thus limiting the efficacy of treatment for tumors and various neurodegenerative diseases. Recently, it was discovered that electroporation (EP) applied in the brain can cause a transient disruption of the BBB lasting for 24–48 h, which may facilitate the uptake of therapeutic agents (Sharabi and Mardor 2016). The exact mechanism of EP-induced BBB disruption is still unclear, but it has been reported to occur at lower thresholds than reversible electroporation of endothelial cells (Sharabi et al. 2019). As with electroporation, BBB disruption is also dependent on electric field strength as well as exposure duration, meaning that the threshold will decrease with increasing exposure duration. The zone of transient BBB disruption is represented in Fig. 2 with a green contour.

EP-induced BBB can be used alone (reversible electroporation only) or in combination with IRE ablation. The latter may be particularly useful in treatment

of brain tumors, where IRE is used to ablate most of the tumor mass, while the area of reversible electroporation and BBB disruption surrounding the ablated tissue is treated with therapeutic drugs to eliminate infiltrating tumor cells while sparing healthy brain tissue (Hjouj et al. 2012; Sharabi et al. 2016).

## 2.7 pH Changes

In recent years new studies have emerged, examining a process previously overlooked in EP-based treatments—the role of pH changes in cell death mechanisms (Turjanski et al. 2011; Maglietti et al. 2013; Olaiz et al. 2014). The theory is based on previous experience in electrochemical treatment of tumors (EChT) where it was shown that two opposing pH fronts emanate from the two electrodes, acidic from the anode and basic from the cathode (Miklavčič et al. 1993), which are related to the extent of the necrotic area (Turjanski et al. 2009). It is suggested that a similar effect may be present in EP-based treatments. While the presence of tissue necrosis is not particularly bothersome in IRE ablation, it is significantly more undesirable in GET. Significant pH changes in the medium can be detrimental to the plasmids used in GET, as DNA denaturation is influenced by pH (Maglietti et al. 2013).

The pH change is attributed to the ion transport, which follows the free diffusion dynamics and is more pronounced at the site of the anode than the cathode (Turjanski et al. 2009). The transport of ions results in strong anodic acidification and cathodic alkalization. A recent *in vitro* study on cell survival and GET efficacy showed, that overall cell survival was better in slightly acidic extracellular conditions, however, the efficacy of GET was decreased (Potočnik et al. 2019).

---

## 3 Tissue Properties and Computation of Electric Field

Different biological tissues have very different dielectric and thermal properties. The dielectric character of tissues is described by electrical conductivity (the ability to transfer electrical charge) and relative permittivity (the ability to store charge and rotate molecular dipoles). Both properties are frequency dependent. Electrical conductivity increases significantly at frequencies above 100 kHz, while permittivity decreases with frequency. However, most EP-based treatments are performed in the lower frequency range, where electrical conductivity can be considered frequency independent, and displacement currents, which are affected by the permittivity, can be neglected. Thermal properties of tissue are mainly characterized by thermal conductivity, specific heat capacity, and tissue perfusion rate. This chapter mainly focuses on the electrical conductivity, since it directly affects the electric field distribution in the target tissue. Nevertheless, some relevant thermal properties are also discussed. At the end of the chapter, the basics of numerical modeling commonly used to study and visualize electric field distribution in tissue are explained as well.

### 3.1 Physiological State of Tissue

There is a large discrepancy in measured values of electrical conductivity reported in literature. Several factors contribute to this variability, for example, tissue inhomogeneity and anisotropy, biological variability, and method of measurement. The physiological state of measured tissue, for instance, pathological changes and whether the measurements were performed *in vivo* or *ex vivo*, also introduce significant variability within the same tissue type.

*In vivo* measurements of dielectric properties are quite challenging; therefore, measurements are often performed *ex vivo* in excised tissue samples. However, the dielectric properties of tissues change rapidly and significantly after death, especially in the lower frequency range (below 1 MHz). For most tissues, the electrical conductivity and permittivity decrease immediately after excision; for example, in liver tissue, the dielectric properties measured *in vivo* can be 16–43% higher than *ex vivo* in the GHz range (O'Rourke et al. 2007).

Pathological changes to tissue, such as the presence of fibrosis in cirrhotic liver and increased fat content in liver steatosis, can have a significant effect on the dielectric properties, due to inherently different cellular architecture (O'Rourke et al. 2007; Peyman et al. 2015). For example, cirrhotic liver has a slightly higher conductivity than normal liver, while liver with steatosis has a lower conductivity due to the low conductivity of fat.

Malignant tissues have significantly different properties from healthy tissue. It is generally accepted, that tumors have higher electrical conductivity than normal tissue (Haemmerich et al. 2009; Laufer et al. 2010; Peyman et al. 2015). This is mainly attributed to altered cell membrane composition and abnormal microvasculature, which results in a presumably higher ion and water content in tumor tissue (Peyman et al. 2015). Laufer et al. (2010) and Haemmerich et al. (2009) measured the conductivity of excised hepatic tumors and normal liver parenchyma. In both studies, the reported conductivity of tumors was approximately 5 times the value of normal liver tissue. The dielectric properties of tumors also vary with the tumor type. For instance, Peyman et al. showed that liver metastases exhibit even higher dielectric properties compared to primary hepatic tumors (HCC), since they originate from a different tissue.

Contrary to dielectric properties, thermal properties are not significantly affected by the pathological changes. Furthermore, changes following death (tissue excision) occur much later than with electrical properties, and are attributed mainly to tissue drying (Duck 2012).

### 3.2 Tissue Anisotropy

Some biological tissues, such as the skeletal muscles, nerves, and bones, exhibit a distinct directional organization of cells and extracellular structures. This allows an easier flow of electric current in a specific direction, meaning that the electrical conductivity of tissue is not equal in all directions. For example in skeletal muscles,

the electrical conductivity parallel to muscle fibers can be up to 5 times higher than the conductivity perpendicular to fiber orientation (Gabriel et al. 2009). Anisotropy may affect the distribution of electric fields in tissue as the electric current preferably flows along the direction with less resistance. At higher frequencies (~1 MHz) the electrical properties become essentially isotropic.

### 3.3 Tissue Perfusion

Tissue perfusion can roughly be divided into microvascular perfusion, which occurs at the capillary level, and macrovascular perfusion, which refers to blood vessels with a diameter greater than 3 mm. Both types of perfusion affect the convective heat transfer; while the well-known heat sink effect is mainly associated with the macrovasculature, microvascular perfusion plays an important role in heat deposition and tissue self-cooling ability (Schutt and Haemmerich 2008). In EP-based treatments, the thermal effects are usually not detrimental, however, in IRE ablation the reduced cooling ability due to vascular effects may impair the nonthermal character of treatment.

The characteristics of tumor vasculature and blood flow are very different from that of normal tissues. Solid tumors are often poorly perfused and oxygenated in comparison with the surrounding tissue, which is generally homogeneously vascularized. Variability in the density of capillaries and oxygenation levels within the tumor volume is often present, abnormal blood vessel walls result in an inferior blood flow regulation and leaky capillaries. These changes contribute to the development of hypoxic regions in the tumor volume and to acidic tissue environment (Jarm et al. 2010). Abnormal tumor blood flow can represent an obstacle for antitumor treatments, as it can impede the interstitial delivery of chemotherapeutic agents. On the other hand, these abnormalities can make the tumor vulnerable due to vascular disrupting effects, present for example in ECT (Cemazar et al. 2001).

### 3.4 Nonhomogenous Tissue

The treated area often consists of more than one tissue type, resulting in a distinct inhomogeneity of tissue properties, especially the electrical conductivity. Examples of tissues with the lowest baseline electrical conductivity are bones, fat tissue, and the outermost layer of the skin (the stratum corneum), while fluids, such as blood and bile, and tissues with a high ionic content, such as the prostate and kidney, have the highest electrical conductivity in the human body (Gabriel et al. 1996, 2009; Duck 2012).

Electric field strength depends on electrical conductivity of the medium (i.e., tissue); therefore, any inhomogeneity in tissue composition needs to be accounted for when calculating the electric field distribution. This is especially important when treating target volumes that contain tissues with significantly different conductivities, as the majority of voltage drop, and consequently electric field

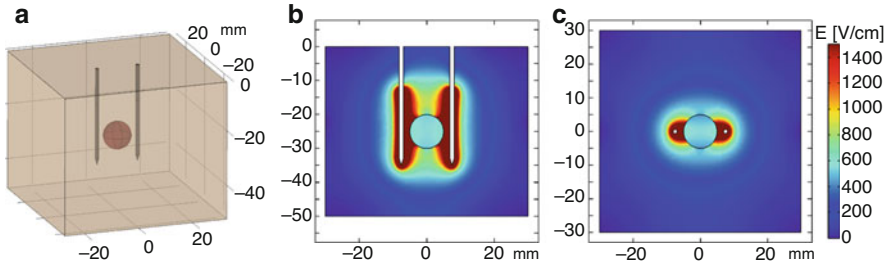


**Fig. 3** A simple numerical model of a deep-seated spherical tumor surrounded by fat (a). Computed electric field distribution in tissue shown in side view (b) and axial view at the largest diameter of the tumor (c). Tumor volume is outlined in black. The baseline electrical conductivity of the tumor is 10 times higher than the surrounding fat tissue. The model parameters are taken from Miklavčič et al. (2010)

strength, occurs in tissues with low conductivity. Examples commonly encountered in clinical practice are deep-seated tumors surrounded by fat tissue (Miklavčič et al. 2010; Denzi et al. 2015) and treatment of subcutaneous tumors through skin (Pavšelj et al. 2005). The stratum corneum presents a major obstacle in transdermal treatment, such as in the case of plate electrodes. Due to its low conductivity, the majority of voltage drop occurs in the skin, and therefore limits the depth of field penetration.

Figure 3 shows a simple model of a deep-seated tumor surrounded by fat tissue. Two needle electrodes are inserted into the tissue 1.5 cm apart and 1500 V is applied to the left electrode. Tumor has a much higher conductivity than fat; therefore, it significantly alters the electric field distribution. We can see on panels B and C, that the electric field strength is lower in the tumor volume than in the surrounding fat. This is due to a higher resistance and the resulting voltage drop in the fat tissue.

### 3.5 Dynamic Tissue Conductivity

Under normal conditions, the cell membrane acts as an electric insulator. During electroporation, the structural changes in the membrane result in the opening of newly formed current pathways, thus increasing the bulk electrical conductivity of affected tissue (Ivorra et al. 2009). The increase in bulk conductivity is generally characterized by a nonlinear dependence on the local electric field. If the electric field strength exceeds the threshold for reversible electroporation, tissue conductivity increases from its baseline value as a function of field strength. If the electric field exceeds a certain threshold, the conductivity increases to its maximum value and does not increase further with the applied electric field (Pavšelj et al. 2005). Various mathematical functions can be used to describe the increase in conductivity, however, the most commonly used are functions of a sigmoid shape (Corovic et al. 2013):

**Table 1** Parameters of tissues composing a simplified model of a subcutaneous tumor

Tissue type	$\sigma_0$ (S/m)	$A$ (-)	$E_1$ (V/cm)	$E_2$ (V/cm)	References
Skin	0.008	100	400	1200	Corovic et al. (2013)
Muscle	0.135	3	200	800	Kos et al. (2010) and Corovic et al. (2013)
Tumor	0.3	3	400	800	Kos et al. (2010) and Corovic et al. (2013)
Fat	0.02	3.5	100	800	Kos et al. (2010)

$$\sigma(E) = \sigma_0 \cdot (1 + \text{sigmoid}(E, E_1, E_2, \sigma_0, A)), \quad (1)$$

where  $\sigma_0$  is the baseline electrical conductivity of target tissue and  $E$  is the local electric field. The shape of the sigmoid function in Eq. (1) is defined by  $E_1$ , which is the electric field threshold at which the conductivity starts increasing,  $E_2$ , which is the electric field at which the conductivity stops increasing, and  $A$ , which is the factor of maximum conductivity increase at electric fields above  $E_2$ .

The dynamics of conductivity increase are not the same for all tissue types. In addition to different baseline conductivity values, the factor of conductivity increase and the respective electric field thresholds are all tissue dependent. Table 1 shows an example of tissue parameters ( $\sigma_0$ ,  $A$ ,  $E_1$ , and  $E_2$ ) used in a simplified model of a subcutaneous tumor. We can see that the fat and muscle conductivities start to increase at a lower electric field than tumor and skin. Furthermore, the factor of increase is much higher for skin than for muscle or tumor, as the outermost skin layer, the stratum corneum, is extremely nonconductive in its unperturbed state. Figure 4 shows the dynamic conductivity as a function of electric field strength [Eq. (1)] for four different tissues shown in Table 1. The thresholds where the conductivity starts to increase ( $E_1$ ) and saturates ( $E_2$ ) are indicated with dashed vertical lines.

Conductivity of biological tissue is also affected by temperature. This is particularly important in IRE where significant heat is produced close to the electrodes. The relationship between electrical conductivity and temperature increase is commonly characterized with a linear equation that assumes a constant temperature coefficient (Rossmanna and Haemmerich 2014):

$$\sigma(T) = \sigma_0 \cdot (1 + \alpha_T \Delta T), \quad (2)$$

where  $\alpha_T$  is the temperature coefficient (rate of increase),  $\Delta T$  is the temperature difference with respect to the initial tissue temperature and  $\sigma_0$  is the baseline electrical conductivity before the increase. Elevated temperature can increase the electrical conductivity even beyond its plateau value caused by the local electric field strength. The dynamic electrical conductivity of tissue is a function of the both electric field and temperature. One example of modelling this co-dependency is by combining Eqs. (1) and (2):

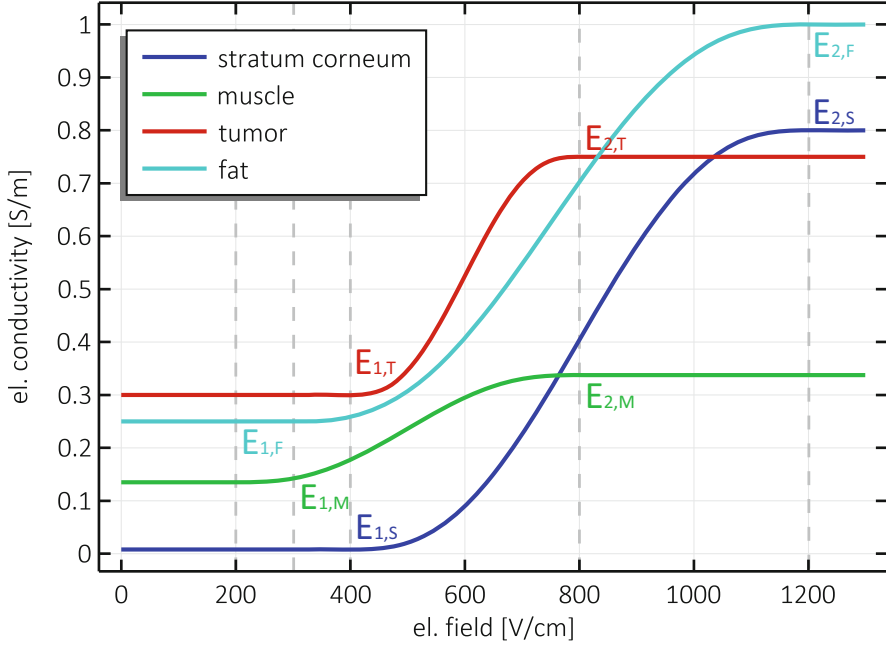


**Fig. 4** The effect of electroporation on the electrical conductivity of various tissues can be approximated with sigmoid functions. The baseline conductivity increases when the applied electric field exceeds the threshold for reversible electroporation. When the irreversible threshold is exceeded, the conductivity reaches its maximum value and does not increase further with increasing field strength. The reversible ( $E_1$ ) and irreversible ( $E_2$ ) thresholds are indicated with dashed vertical lines (S—stratum corneum, M—muscle, T—tumor, F—fat). The baseline conductivities, factors of conductivity increase, and respective thresholds are taken from Kos et al. (2010 and Corovic et al. (2013) and are summarized in Table 1

$$\sigma(E, T) = \sigma(E) \cdot (1 + \alpha_T \Delta T), \quad (3)$$

where  $\sigma(E)$  represents the nonlinear increase due to electroporation effect. Other approaches to modelling the combined thermal and electroporation effects are reported in literature, since it is difficult to decouple the two mechanisms (Garcia et al. 2011; Zhao et al. 2020).

### 3.6 Numerical Computation of Electric Field Distribution in Tissue

To achieve a therapeutic effect, complete coverage of target tissue volume with sufficiently high electric field is required in all EP-based treatments. Due to tissue-specific properties and various electrode geometries and pulse parameters used in treatments, the distribution of electric field is often not easy to determine. Numerical modelling is an effective way of predicting the shape and strength of the applied

electric field for a selected set of parameters, electrodes, and target tissues. It is based on constructing a simplified anatomical model of the target tissue and solving a set of algebraic equations using the finite element method. The most common numerical models of electroporation are based on solving the partial differential equation for electric potential in stationary conditions (Šel et al. 2007; Pavšelj and Miklavčič 2008; Županič et al. 2012):

$$\nabla \cdot (\sigma \nabla V) = 0, \quad (4)$$

$$E = -\nabla V, \quad (5)$$

where  $V$  is the electric potential,  $\sigma$  is the tissue conductivity and electric field  $E$  is defined as the gradient ( $\nabla$ ) of electric potential. Most EP-based treatments use 50–100 $\mu$ s long pulses, which means all transient phenomena of electroporation will have settled long before the end of the pulse, and steady-state conditions can be used for computation. The electrical conductivity change during electroporation is implemented in the model in the form of a nonlinear function of the local electric field strength [Eq. (1)].

The initial step in numerical modelling is constructing the model geometry that reflects the patients' conditions as closely as possible. For treatment planning complex geometries are constructed based on patients' medical images (Grošelj et al. 2015; Kos et al. 2015), however, for investigative purposes (such as in this chapter) simplified geometries are used, where tumors are usually represented by spheres or spheroids surrounded by blocks of healthy tissue of sufficiently larger dimensions. The appropriate electrode geometry is built on the model in the form of voltage terminals; for deep-seated tumors needle electrodes are generally used, while for superficial tumors plate or various fixed array electrodes are used. When the geometry is defined, voltage is applied to the electrodes and electric potential and field are computed in the whole model domain according to Eqs. (4) and (5). The model complexity can be further increased by including additional anatomical objects, such as nearby vessels and tissue layers, and by including tissue anisotropy and inhomogeneity (Kos et al. 2010, 2015).

If thermal effects need to be investigated, for example, in IRE ablation, the computation needs to be transformed from stationary conditions to time domain. Thermal effects are most commonly modelled by the modified Pennes' bioheat equation (Pennes 1948; Agnass et al. 2020):

$$\rho C \frac{\partial T}{\partial t} = \nabla(k \nabla T) - Q_{\text{perf}} + Q_{\text{met}} + \sigma |E|^2, \quad (6)$$

where  $\rho$ ,  $C$  and  $k$  are density, thermal capacity, and thermal conductivity of tissue, respectively,  $T$  is tissue temperature,  $t$  is time,  $Q_{\text{perf}}$  is the blood perfusion term,  $Q_{\text{met}}$  is the metabolic heat generation term and  $\sigma |E|^2$  is the Joule heating term. In this case the nonlinear conductivity function is a function of electric field and temperature [Eq. (3)].

## 4 Electrode Designs and Configurations

Different therapeutic needs necessitate the development of different electrode types and models; from noninvasive electrodes intended for transdermal treatment to various needle electrodes with fixed or variable geometry for treatment of superficial or deep-seated tumors. Finger and small cavity electrodes have been developed for treatment in hard-to-reach locations, for example, in the oral cavity. Special electrode designs are continuously being developed for treatment of specific organs; for instance, thicker needle electrodes (1.8 mm instead of standard 1.2 mm diameter) with a trocar tip intended to penetrate the rigid bone tissue (Miklavčič et al. 2012), or electrodes with internal cooling to reduce heating during IRE ablation (O'Brien et al. 2018). In this section, a few examples of commercially available electrodes are shown, although new electrode models are being studied and developed for clinical use. Some examples of most commonly used electrode types in current clinical practice are also illustrated with simple numerical models to show the expected electric field distribution in tissue.

### 4.1 Noninvasive Electrodes

Noninvasive electrodes mainly consist of various types of plate and L-shaped electrodes and are intended for the treatment of skin and small superficial tumor nodules, e.g., various skin metastases. These electrodes cannot be inserted into the tissue, so the skin must be considered when evaluating the treatment response. Conductive gels are often used to provide better electrical contact between the electrodes and skin surface.

The plate electrode (Fig. 5a) was most commonly used in early studies of electrochemotherapy (Miklavčič et al. 2014). Due to a simple geometry consisting of two parallel plates, the electric field was most often estimated as the ratio between the applied voltage and the distance between the inner surfaces of the plates. However, this simplification is only valid if the distance between the electrodes is much smaller than their surface area and if the target tissue is homogenous with electrical conductivity independent of the applied electric field, which is not to be expected in a real clinical application. The electric field strength depends on the thickness and conductivity of the tissue in question, but generally, the tissue with lower conductivity (e.g., skin) experiences a higher electric field. Figure 6 shows the electric field distribution in a simple model of a skin fold treated with plate electrodes with 8 mm spacing. With this type of electrodes  $8 \times 100\mu\text{s}$  pulses are delivered with a pulse repetition rate of 5000/s with the suggested pulse amplitude of 960 V, resulting in a voltage-to-distance ratio of 1200 V/cm. Due to an inhomogeneous tissue and dynamic electrical conductivity, the actual electric field experienced by the tissue is less than 1200 V/cm as can be seen in Fig. 6. The strongest electric field is found in the outer layer of skin at the surface of the electrodes and decreases with distance from the electrodes. For this reason, the distance between the electrodes must be small compared to their surface area. Panels c and d in Fig. 6 show the

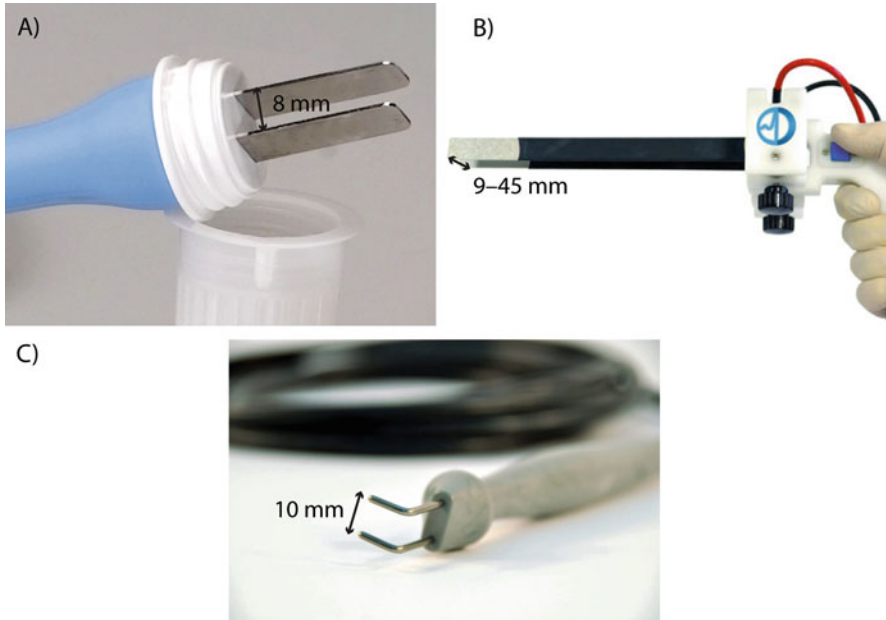


**Fig. 5** Examples of noninvasive electrodes. (a) A plate electrode with a fixed spacing for clinical use (P-30-8B, EPS Series, IGEA S.p.A., Italy). (b) Clamp plate electrode with adjustable spacing for veterinary use (M1 Clamp, OnkoDisruptor, Biopulse Biotech, Italy). (c) L-shaped electrode for veterinary use (ELECTROvet, Leroy Biotech, France)

skinfold model with added small tumor nodule (4 mm diameter). The electric field distribution is affected by the higher conductivity of the tumor compared to surrounding fatty tissue.

The main advantages of plate electrodes are their noninvasiveness and a relatively easy visualization of the area treated by electric field. However, the applicability of plate electrodes is limited to small superficial areas, such as earlobes, nose, or superficial exophytic tumor nodules that can be compressed between the plates. In addition to plate electrodes with fixed spacing, clamp plate electrodes with adjustable spacing (Fig. 5b) have also been developed for veterinary electrochemotherapy of tumors of various sizes. L-shaped electrodes are also used for treatment of skin and small superficial tumors (Fig. 5c). Multiple applications are generally advised with the rotation of the electrode for 90 degrees in between, in order to treat the target tissue from all directions (Serša et al. 1996). With the L-shaped electrode shown on Fig. 5c,  $4 \times 100\mu$  pulses of 1300 V amplitude are applied in each position. In all noninvasive electrode models, the depth of effective electric field penetration is very limited—usually to only a few millimeters from the surface.

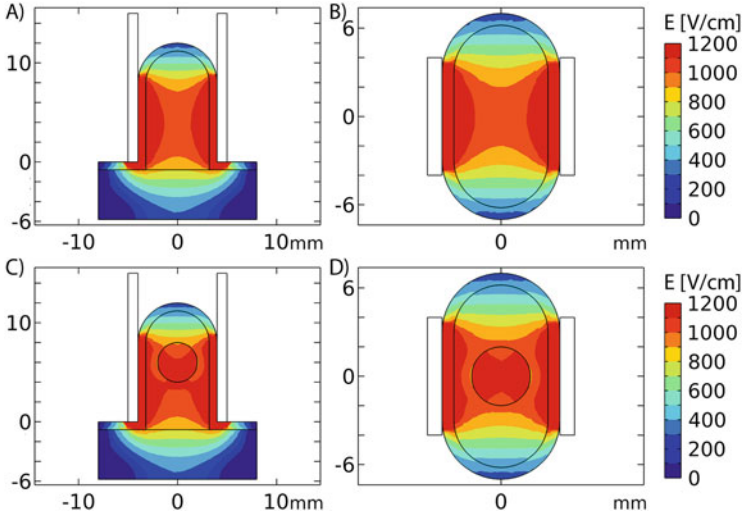


**Fig. 6** Electric field distribution with plate electrodes in side view (a, c) and axial view (b, d). Panels (a) and (b) show a simple skinfold model, consisting of skin and fat. Panels (c) and (d) show the same model with the addition of a tumor with a 4 mm diameter. The distance between the plates is 8 mm and applied voltage is 960 V, resulting in a voltage to distance ratio of 1200 V/cm. Due to an inhomogeneous tissue and a dynamic electrical conductivity, the actual electric field experienced by the majority of tissue volume is lower than 1200 V/cm (dark red contour). The electric field is strongest in the skin layer due to its low conductivity and immediate proximity to the electrode surface. The addition of tumor volume (c, d) alters the field distribution even further. The color scale is adjusted to the range of up to 1200 V/cm for better visibility

## 4.2 Needle Electrode Arrays (Fixed Geometry)

Needle electrodes with a fixed geometry are the most commonly used electrode type in ECT. Unlike non-invasive electrodes, needle electrodes must be inserted into the tissue. Figure 7, panels a–d show some of the commercially available needle electrodes with fixed geometry. Although there are many possibilities, the most common models have either a linear (Fig. 7a, b) or a hexagonal (Fig. 7c) needle configuration and are used for treatment of superficial tumors. Figure 7d shows a different design of a needle electrode, intended for endoscopic and laparoscopic uses. The electrode has a flexible shaft with a modular needle exposure and is designed for minimally invasive treatment of lesions localized in the abdominal parenchyma.

The most common model of linear needle electrodes consists of two rows of four needles, separated by 4 mm (Fig. 7a). The needles of each row are connected together, therefore, the electrical connection of the electrode is effectively bipolar (Bertacchini 2017). Fixed linear electrodes are used for treatment of smaller tumor nodules. Typically  $8 \times 100\mu\text{s}$  pulses are delivered with a pulse repetition rate of 5000/s and pulse amplitude of 400 V. Figure 8 shows an example of the electric field

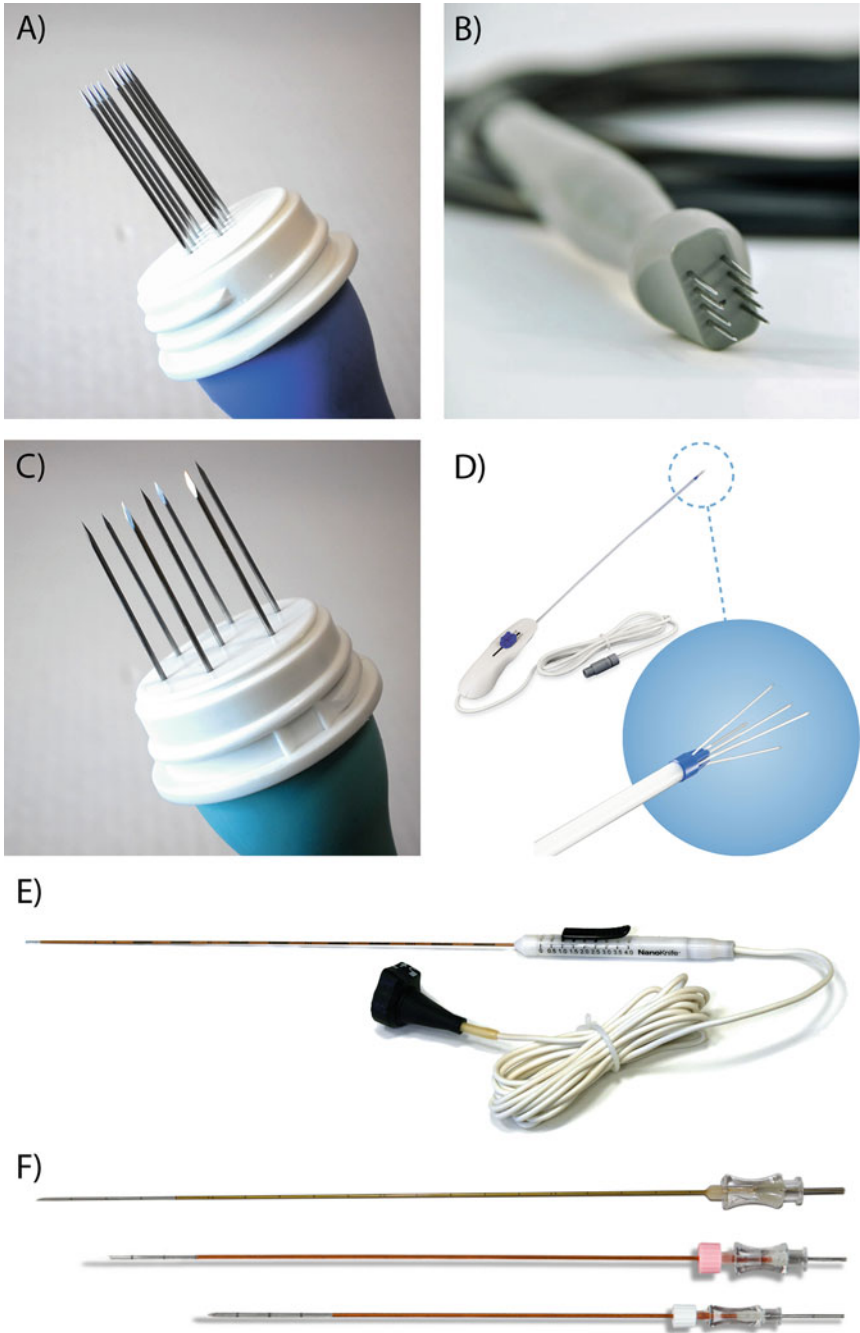


**Fig. 7** Examples of needle electrodes. (a) Electrode array with a fixed linear geometry (4 mm spacing) for clinical use (N-xx-4B, EPS Series, IGEA S.p.A., Italy). (b) Electrode array with a fixed linear geometry (5.9 mm spacing) for veterinary use (ELECTROvet, Leroy Biotech, France). (c) Electrode array with a fixed hexagonal geometry for clinical use (N-xx-HG, EPS Series, IGEA S.p.

distribution using a linear electrode in a homogenous tissue model (a, b) and nonhomogeneous tissue model (c, d)—a subcutaneous tumor of 6 mm diameter.

Hexagonal electrodes consist of six needles distributed in a hexagonal configuration around the central (seventh) needle. In the electrode model shown in Fig. 7c, the distance between the needles is 7.3 mm, resulting in cylindrically shaped treatment area with an approximately 15 mm diameter. This geometry enables the treatment of larger tumor nodules compared to linear electrodes. Typically  $8 \times 100\mu\text{s}$  pulses (4 + 4 with reversed electrode polarity) are delivered with the pulse repetition rate of 5000/s and 730 V amplitude to each needle pair individually. The seven needles form together 12 unique electrode pairs, resulting in 96 total pulses delivered in a single application. Figure 9 shows an example of the electric field distribution using a hexagonal electrode in a homogenous tissue model (a, b) and nonhomogeneous tissue model (c, d)—a subcutaneous tumor of 12 mm diameter.

For both electrode models, the needle length can be adjusted from 10 to 40 mm. The depth of electrode insertion dictates the depth of penetration of electric field. However, with longer electrodes (longer electrode exposure), higher electric currents are to be expected during treatment, i.e., the current amplitude depends on the depth of electrode insertion. With fixed needle electrodes the electric field distribution is more complex than with plate electrodes, since pulses are applied to multiple electrode pairs and in different directions. Nevertheless, the geometries and necessary parameters have been extensively studied, therefore, the user needs only to ensure the treated tumor is contained within the needle boundaries (Bertacchini 2017). For larger tumors, multiple applications with repositioning of the electrodes are often performed (for both linear and hexagonal configurations).

### 4.3 Single Needle Electrodes (Variable Geometry)

For minimally invasive treatment of deep-seated tumors, single monopolar needle electrodes are used in pairs to deliver high-voltage electric pulses to target tissue. Single needle electrodes are the most versatile electrode type, however, their placement is challenging and requires an experienced interventional radiologist (Rossmesl et al. 2015; Garcia et al. 2017). Moreover, given the limitations of available pulse generators in terms of maximum voltage and electric current delivery, the treatment typically requires the use of more than one pair of electrodes, further complicating the determination of the electric field distribution in the tissue. Nevertheless, even a single electrode pair allows effective coverage of larger tissue volumes than other electrode types. The number and placement of electrodes depend on the size of the tumor, but typically 3–6 electrodes are used in a polygonal

---

**Fig. 7** (continued) A., Italy). (d) A flexible electrode with modular needle exposure for endoscopic and laparoscopic use (Stinger, EGPS Series, IGEA S.p.A., Italy). (e) Single needle electrode for IRE ablation of deep-seated tumors (NanoKnife, Angiodynamics Inc., USA). (f) Single needle electrodes for ECT of deep-seated tumors (VGD Series, IGEA S.p.A., Italy)

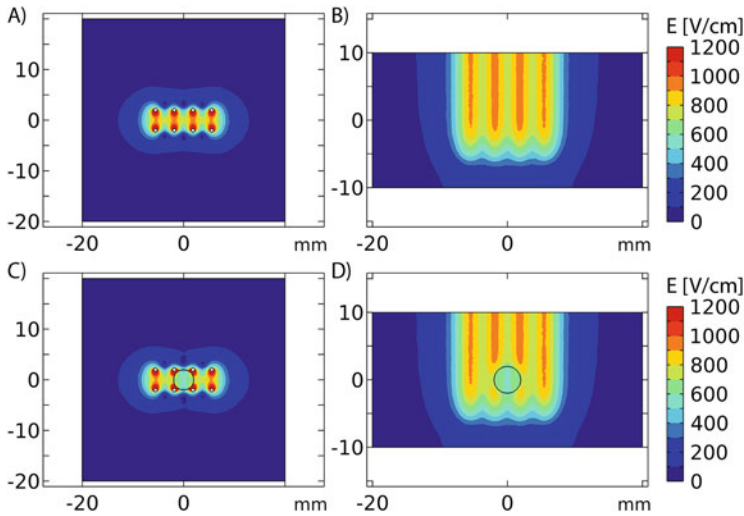


**Fig. 8** Electric field distribution in homogenous (a, b) and nonhomogeneous (c, d) tissue model using the fixed linear needle electrodes. In the nonhomogeneous model a spherical tumor with 4 mm diameter is positioned in the center of electrode geometry (black outline). The distance between the rows is 4 mm, insertion depth is 15 mm and the applied voltage is 400 V, as is recommended for ECT with this electrode type, resulting in a voltage to distance ratio of 1000 V/cm. Dynamic electrical conductivity is used in both models. In the nonhomogeneous model, the tumor conductivity is approximately 3-times the value of surrounding tissue conductivity. The color scale is adjusted to the range of up to 1200 V/cm for better visibility. Panels (a) and (c) show the axial view at the depth of the largest tumor diameter. Panels (b) and (d) show the side view in the middle between the needle rows

configuration in close proximity or even inside the tumor mass. The electrodes should be positioned parallel to each other and at the same depth to achieve a predictable electric field shape. In practice, this is often difficult to achieve due to anatomical constraints; moreover, the electrodes are long and thin and tend to bend. The electrodes also have an adjustable active length (1–4 cm), but in practice 2 cm are usually used, because longer electrodes result in a (too) high electric current, which may cause automatic termination of pulse delivery by the pulse generator.

The electric field is the strongest in immediate vicinity of the electrode and decreases rapidly with distance from the electrode. The proximity of the counter electrode in the pair is crucial in establishing the necessary field strength in the whole target volume. Figure 10 illustrates the effect of inter-electrode distance on the electric field distribution in a simple model with two needle electrodes in a homogeneous tissue. A fixed voltage-to-distance ratio of 1500 V/cm is used to determine the applied voltage, as this value is most commonly recommended for IRE treatment of deep-seated tumors. The distance between the electrodes is set to either 1 cm, 1.5 cm or 2 cm. At 1 cm distance, the electric field appears almost homogenous in the middle between the electrodes with a strength of approximately 1200 V/cm. When

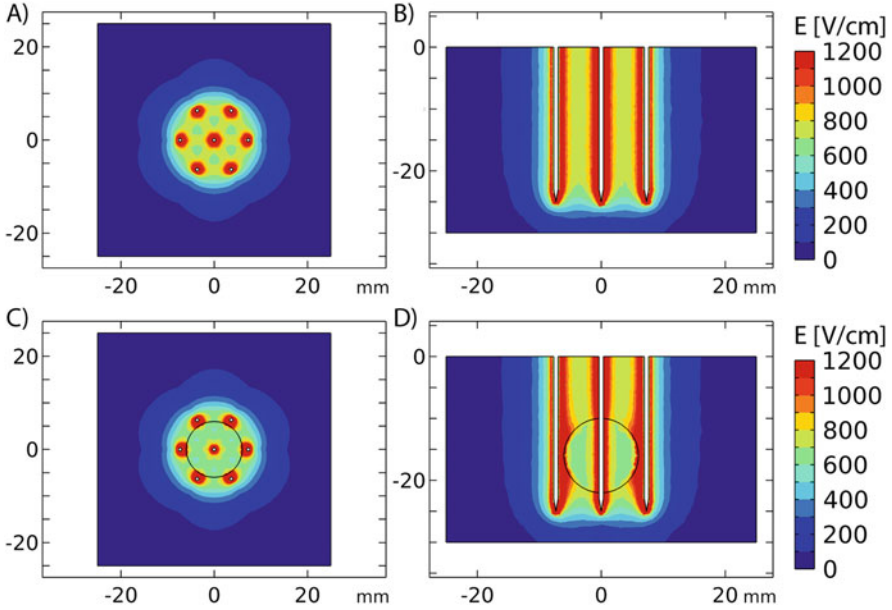


**Fig. 9** Electric field distribution in homogenous (a, b) and nonhomogeneous (c, d) tissue model using the fixed hexagonal needle electrodes. In the nonhomogeneous model, a tumor with 12 mm diameter is positioned in the center of electrode geometry (black outline). The distance between the needles is 7.3 mm, insertion depth is 25 mm and the applied voltage is 730 V, as is recommended for ECT with this electrode type, resulting in a voltage to distance ratio of 1000 V/cm. Dynamic electrical conductivity is used in both models. In the nonhomogeneous model, the tumor conductivity is approximately 3-times the value of surrounding tissue conductivity. The color scale is adjusted to the range of up to 1200 V/cm for better visibility. Panels a and c show the axial view at the depth of the largest tumor diameter. Panels b and d show the side view at the central electrode aligned with the  $x$ -axis

the electrodes are positioned further apart, the electric field strength in the middle decreases and becomes more inhomogeneous. To compensate for this decrease, a higher voltage needs to be applied to the electrodes; however, the maximum voltage that can be supplied by the currently approved medical pulse generators is limited to 3000 V, therefore limiting the distance between the electrodes. For example, the general guideline for IRE ablation is that the electrodes should not be further than 2 cm apart to ensure the recommended voltage-to-distance ratio of 1500 V/cm.

A fixed voltage-to-distance ratio is usually suggested by the manufacturer of the pulse generator, as a guideline for determining the voltage applied to the electrodes. However, the applied voltage can then be adjusted by the user. In literature, the voltage-to-distance ratio is often confused with the electric field threshold, required for electroporation, as both have the same unit of measure—V/cm. The recommended voltage-to-distance ratio is much higher than the necessary threshold for electroporation, to compensate for the decrease in field strength with distance.

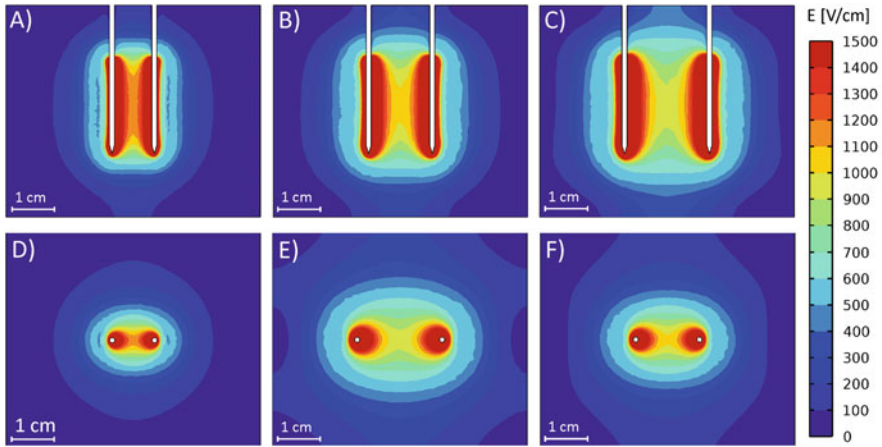


**Fig. 10** An example of electric field distribution in homogeneous tissue at different distances between needle electrodes—1 cm (**a, d**), 1.5 cm (**b, e**), and 2 cm (**c, f**). A fixed voltage-to-distance ratio of 1500 V/cm was used to determine the applied voltage. The active length of the electrodes was 2 cm. The electric field is strongest in the immediate vicinity of the electrodes, but decreases rapidly with the distance from the electrode surface. For better visibility, the color scale is adjusted to a range of up to 1500 V/cm, however, very high electric fields (up to 10,000 V/cm) can be found in tissue directly at the electrode surface

For instance, in Fig. 10 the voltage-to-distance ratio was set to 1500 V/cm. However, we can see that the 1500 V/cm field strength (dark red contour) only occurs in a few millimeters from the electrodes, while in most of the tissue between the electrodes the field strength is considerably lower.

According to manufacturer instructions, the electrodes should be placed parallel to each other and at the same depth, since it is easier to predict the distribution and homogeneity of the resulting electric field. However, in biological tissues this placement is almost impossible to achieve, due to electrode bending and anatomical constraints. Any imperfections in the electrode positions result in a much more complex distribution of electric field. Figure 11 shows the effect of electrode angulation and skewness on the shape of the electric field in a homogeneous tissue. In a clinical setting some angulation and skewness, as shown in panel d of Fig. 11, is to be expected. Examples shown in Figs. 10 and 11 are computed in a homogeneous tissue with dynamic conductivity. In reality, biological tissue is inhomogeneous considering its conductivity, and any inhomogeneity in target tissue properties alters the electric field distribution even further.

#### 4.4 Finger/Cavity Electrodes

In some anatomical locations, for instance some orifices and cavities, standard electrodes could not be used. Therefore, electrodes have been designed shaped specifically for treatment in these challenging locations. Figure 12 shows two

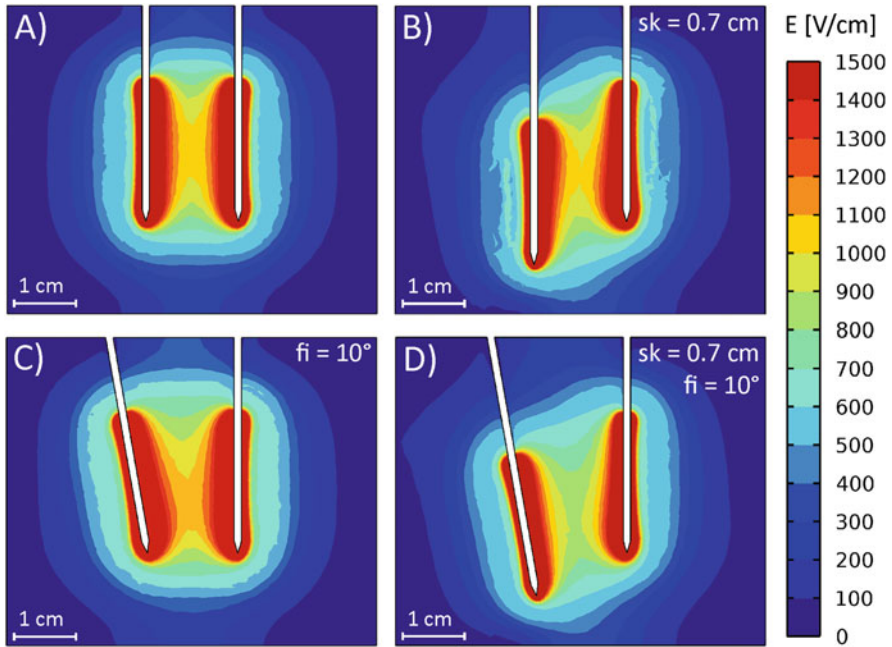


**Fig. 11** The effect of electrode skewness and angulation on electric field distribution in homogeneous tissue. A fixed voltage-to-distance ratio of 1500 V/cm was used to determine the applied voltage. The active length of the electrodes was 2 cm. **(a)** Ideal placement—parallel electrodes, same depth of insertion. Distance between the needles is 1.5 cm. **(b)** Parallel electrodes, left electrode is placed 0.7 cm deeper. **(c)** Same depth of insertion, left electrode is inserted at a 10° angle with respect to the vertical axis of insertion. **(d)** Left electrode is inserted at an angle and deeper than the counter electrode. This scenario is most commonly encountered in clinical practice

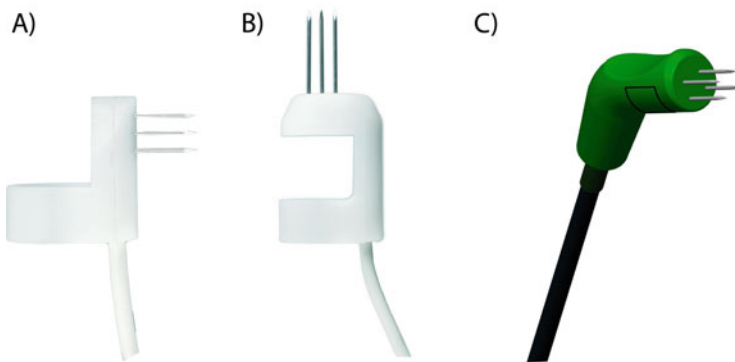


**Fig. 12** Examples of electrodes for treatment in locations with difficult access. **(a)** Orthogonal model (F-15-NO, NFD Series, IGEA S.p.A., Italy) and **(b)** longitudinal model (F-xx-NL, NFD Series, IGEA S.p.A., Italy) of a finger electrode with linear needle configuration for treatment in the human orifices. **(c)** Cavity electrode, designed specifically for treatment in the oral cavity in veterinary oncology (ELECTROvet, Leroy Biotech, France)

models of finger electrodes, designed for ECT treatment in the human orifices. As the name suggests the electrode is to be worn on the finger of the user and has the linear needle configuration. The distance between the rows is 4 mm while the active length can be either 5 or 10 mm. The needles can be positioned either perpendicular to the finger (orthogonal model) or at the tip of the finger (longitudinal model) to allow treatment of difficult-to-reach sites (Bertacchini 2017; Campana et al. 2019). Panel c of Fig. 12 shows a cavity electrode, designed for ECT of tumors in the oral cavity of animal patients, which consists of four 10 mm long needles.

---

## 5 Pulse Parameters (Treatment Protocols)

Electroporation-based treatments have different needs regarding the desired therapeutic effect and therefore require the use of pulse parameters and delivery protocols, tailored to each type of treatment. The classical electroporation protocol of  $8 \times 100\mu\text{s}$  pulses, developed in the first studies of electrochemotherapy, is still the most widely used protocol in clinical practice, however, several new protocols have also been developed.

### 5.1 Electrochemotherapy

Electrochemotherapy (ECT) uses reversible electroporation to facilitate transmembrane transport of chemotherapeutic agents with intercellular action, e.g., bleomycin and cisplatin. The most widely known ECT protocol consists of 8 pulses of  $100\mu\text{s}$  duration and a pulse repetition rate of 1/s (Mir et al. 1991). In some commercially available devices today, such as the Cliniporator (IGEA S.p.A., Italy), the protocol is adjusted so the pulses are no longer delivered at 1/s, but rather in trains of pulses with a pulse repetition rate of 5000/s. For treatments in the thoracic region, the train delivery is synchronized with the patients' electrocardiogram to prevent cardiac arrhythmias. With a pulse repetition rate of 1/s, each of the eight delivered pulses manifests as separate muscle contraction perceived by some patients as painful. By increasing the pulse repetition rate the patient effectively experiences only a single pulse instead of eight, which decreases the unpleasantness of the procedure (Zupanic et al. 2007). The most commonly used electrode models in ECT are the fixed linear and hexagonal needle electrodes for treatment of skin and subcutaneous tumors. Both electrode models come with recommendations for applied pulse parameters, namely the applied voltage, provided by the device manufacturer.

### 5.2 Irreversible Electroporation Ablation

Irreversible electroporation (IRE) is used as a focal ablation method for various soft tissues and tumors. In IRE ablation, a higher number of monopolar pulses is used compared to ECT. Parameters of electric pulses and supply protocols differ between

studies, but 70–100 electric pulses per electrode pair are most commonly used, and the duration of individual pulses in the train is 50–100 $\mu$ s. The pulse delivery is synchronized with the patients' electrocardiogram, so the pulses are delivered in the absolute refractory period to minimize the risk of triggering arrhythmias. In current pulse generators, sequences of 10 pulses are applied, followed by a short pause to allow recharging of the generator. The pulse amplitude is most often determined by using a fixed ratio between the applied voltage and the distance between paired electrodes.

The most recent development in pulse protocols for IRE is the so-called high-frequency IRE or H-FIRE (Arena et al. 2011; Yao et al. 2017; Ringel-Scaia et al. 2019). In H-FIRE, bursts of bipolar pulses are applied instead of monopolar pulses used in classic electroporation protocols. The bipolar pulses consist of two pulses of opposite polarity. The duration of a single polarity pulse is in the range of a few microseconds and the pulse repetition rate is in the range of 50,000–125,000/s. The short duration of the pulses and higher repetition rates provide several benefits over longer monopolar pulses, such as a higher threshold for nerve and muscle stimulation.

### 5.3 Gene Electrotransfer

Gene electrotransfer (GET) uses electrical pulses to introduce gene-encoding plasmid DNA into tumor or healthy cells, for example, to induce an antitumor effect or stimulate the immune response (Gothelf and Gehl 2010; Heller and Heller 2015; Rosazza et al. 2016; Lamprecht Tratar et al. 2017). As in ECT, the DNA plasmid is injected into the target tissue a few seconds before the pulse application. Unlike the chemotherapeutics in ECT, plasmid DNA molecules are too large to enter the cell by diffusion. Therefore, longer (millisecond range) low-voltage pulses, or a combination of short (microsecond range) high-voltage pulses and long (millisecond range) low-voltage pulses are used to permeabilize the cell membrane and electrophoretically deliver the plasmid to the target location (Gothelf and Gehl 2010). The optimal dose of the plasmids and pulsing protocols are still under development.

### 5.4 Additional Considerations Regarding Pulse Protocols

Sometimes the recommended pulse parameters cannot be delivered, for instance, due to the limitations of available equipment or specific properties of the experimental setup. Studies have shown that a similar therapeutic outcome can be achieved also with somewhat adjusted pulse parameters (Pucihar et al. 2011; Dermol and Miklavčič 2015; García-Sánchez et al. 2019). For example, at a fixed field amplitude, a similar fraction of electroporated cells can be obtained by using longer pulses or a higher number of pulses. In other words, with longer pulses or higher number of pulses, the critical electric field thresholds shift to lower values (also see Fig. 1). In order to select equivalent pulse parameters, the relations between the pulse

amplitude, duration, and number need to be determined. In their experimental study, Pucihar and colleagues (Pucihar et al. 2011) determined the mathematical relations between amplitude and pulse duration and amplitude and number of delivered pulses with respect to the fraction of electroporated cells in vitro. The results of their study show, that the relations between pulse parameters can be reflected by rather simple mathematical models and that a similar fraction of electroporation can indeed be achieved using carefully selected equivalent parameters.

Pulse delivery dynamics, namely the duration of pulses and pulse repetition rate, also play an important role in tissue heating. The thermal energy  $W_T$  is formulated as the product of power (electrical energy converted to thermal energy per unit time) and time:

$$W_T = P \cdot t = \left( \int_V \mathbf{J} \cdot \mathbf{E} \, dv \right) \cdot t = \left( \int_V \sigma \cdot E^2 \, dv \right) \cdot t \quad (7)$$

where  $P$  is power,  $t$  is time (pulse duration),  $J$  is current density,  $E$  is electric field,  $\sigma$  is electrical conductivity of the tissue. The main factor driving the amount of generated thermal energy is the pulse amplitude and the associated Joule heating [ $\mathbf{J} \cdot \mathbf{E}$  term in Eq. (7)] (Lacković et al. 2009). However, as we can see in Eq. (7), the amount of thermal energy also depends on the duration of the applied pulses. There is a considerable difference between the amount of thermal energy generated by a millisecond pulse and a nanosecond pulse of an equivalent amplitude. Living tissue also has the ability to diffuse heat due to micro- and macrovascular perfusion. Tissue cooling effectively happens in the pauses between the individual pulses. If the tissue capacity to effectively diffuse heat after a single pulse is exceeded the tissue temperature will begin to increase. Longer pauses between the pulses (lower pulse repetition rate) result in more effective cooling. However, due to vascular effects of electroporation, the perfusion and therefore the tissue cooling ability is greatly diminished. This is especially important in IRE ablation, where several hundreds of pulses are cumulatively delivered to tissue, resulting in a large amount of generated heat. Strategies for decreasing the thermal effects are being investigated by the use of electrodes with internal cooling or development of protocols, where pulses are delivered in groups with long delays in between (O'Brien et al. 2018; Sano et al. 2020).

---

## 6 Numerical Prediction of Treatment Outcome (Treatment Planning)

### 6.1 Cumulative Coverage of Target Tissue

The volume of tissue that can be effectively treated with a single electrode pair is rather small, therefore, multiple electrodes (electrode pairs) are used in EP-based treatments—be it the fixed electrode models consisting of multiple needles (Figs. 8 and 9) or multiple single needle electrodes (Figs. 10 and 11). In such cases pulses are

delivered to electrode pairs in sequence, therefore, the target tissue volume is cumulatively covered by contributions from all active electrode pairs. The most conservative method for evaluating cumulative coverage of the target tissue is by considering each of the electrode pairs as a separate entity and superimposing their respective contributions as the treatment equivalent field  $E_{\text{eq}}$ :

$$E_{\text{eq},n} = \begin{cases} \max(E, E_{n-1}); n > 1 \\ E_n; n = 1 \end{cases}; 1 \leq n \leq N, \quad (8)$$

where  $N$  is the total number of electrode pairs,  $E_{\text{eq},n}$  is the treatment equivalent field after application of pulses to the  $n$ th electrode pair,  $E_{\text{eq},n-1}$  is the treatment equivalent field from electrode pairs 1 to  $n - 1$  and  $E_n$  is the actual computed electric field produced by the  $n$ th electrode pair. The final electric field distribution in tissue is represented by the equivalent electric field after application of pulses to all  $N$  electrode pairs— $E_{\text{eq},N}$ . This approach is illustrated in Fig. 13 showing a spherical tumor model treated with four needle electrodes forming a total of six unique electrode pairs. A threshold of 600 V/cm (often used as the threshold for IRE of tumors) is applied to the computed electric field, so the Panels a–f show only tissue covered in electric field strength of or above this threshold. The tumor volume is gradually covered in six segments and the final electric field distribution is shown in panel g. Figure 14 shows the fraction of tumor volume cumulatively covered by pulses sequentially delivered to each of the electrode pairs.

When using more than one electrode pair some areas of tissue will be covered more than once, as can be seen in panels a–f of Fig. 13 (darker blue areas, mainly around the electrodes). This is also very prominent in the hexagonal electrodes, where the central needle serves as the counter electrode in half of all active electrode pairs (6 out of 12 pairs), while each of the outer needles is only used in 4 out of 12 pairs. The tissue surrounding the central electrode will therefore cumulatively experience twice as many pulses as the tissue at the electrode rim.

Considering each pair of electrodes individually will slightly underestimate the extent of the treated region. First, the conductivity increase is not completely independent between the pairs, as a small increase persists also during the time when the pulse delivery is switched to the next pair. Moreover, the required electric field strength to achieve reversible or irreversible electroporation in the target volume reduces with increased exposure duration (see also Fig. 1 and Sect. 5.4). Therefore, in tissue areas that are cumulatively experiencing a higher number of pulses, electroporation may occur already at a lower electric field than expected (Pucihar et al. 2011).

Another possible approach to determine the tissue response is by calculating the probability of effective electroporation in tissue volume. This approach employs the use of statistical models of cell survival, the most commonly used being the Peleg-Fermi model (Peleg 1995; Golberg and Rubinsky 2010; Dermol and Miklavčič 2015). The probability of cell survival  $S$  is defined as follows:

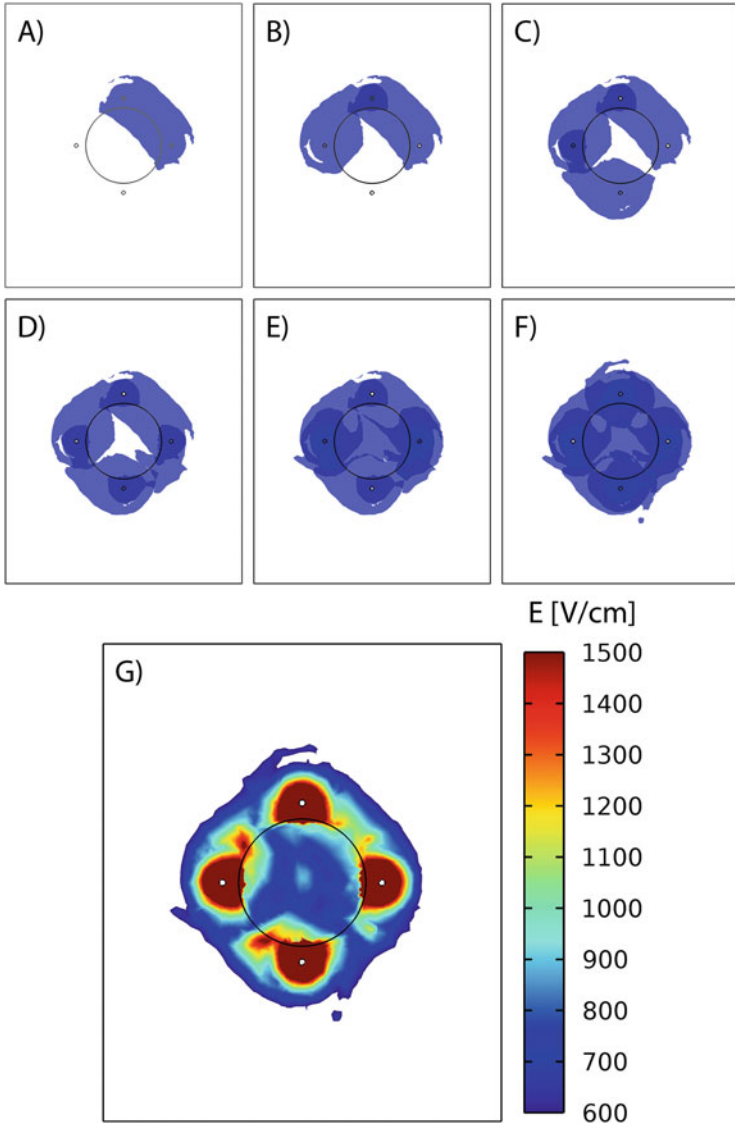


**Fig. 13** A simplified model of IRE ablation of a subcutaneous tumor. Four electrodes are used in the model, forming six unique electrode pairs. The tumor volume is gradually covered with electric field at or above the irreversible threshold—in this case 600 V/cm. Panels (a–f) show the volume of target tissue covered by at least 600 V/cm after application of pulses to each electrode pair. Panel (g) shows the final electric field distribution in the target tissue. The round contour of the tumor can be seen. The color scale is adjusted to the range of 600 to 1500 V/cm for better visibility

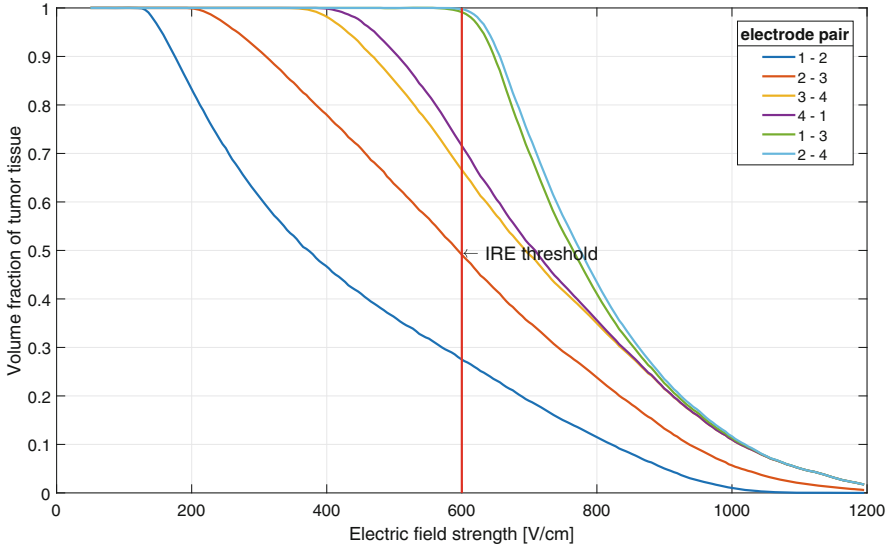


**Fig. 14** Cumulative coverage of the tumor volume with electric field. The horizontal axis shows the electric field strength, while the vertical axis shows the fraction of tumor volume covered with electric field of at least the value shown on the horizontal axis. Each curve represents the contribution of a single active electrode pair used in treatment. The critical value for the therapeutic response in this specific case is the IRE threshold of 600 V/cm, however, this value depends on the tissue type and treatment application

$$S(E, m) = \frac{1}{1 + \exp\left(\frac{E - E_c(m)}{A(m)}\right)}, \quad (9)$$

where  $m$  is the number of pulses,  $E$  is the local electric field,  $E_c(m)$  is the critical electric field at which 50% of affected cells die, and  $A(m)$  is the shape factor defining the size of the transition zone. Both the critical field and shape factor are functions of applied pulse number. There are two main benefits of this approach; the number of applied pulses is included in the calculation, and the nature of probability calculations allows multiplication of different probabilities to reflect the lower probability of survival, where applicable:

$$S = \prod_{N \text{ pairs}} S_n, \quad (10)$$

where  $S_n$  is the probability of cell survival after the application of pulses to the  $n$ th electrode pair. Considering Eq. (10), the cumulative probability of cell survival will be lower in tissue areas that are covered with multiple pairs.

The last aspect to consider when looking at cumulative coverage is the thermal effects. As the number of delivered pulses increases, the thermal component becomes more pronounced. In IRE ablation, up to 100 pulses are delivered to a

single pair of electrodes. Combining the contributions of all active electrode pairs, certain tissue areas are cumulatively exposed to several hundred pulses. Due to slow thermal diffusion in tissue and ineffective blood perfusion during electroporation a significant thermal component is present (Cornelis et al. 2020). This effect cannot be neglected even in reversible electroporation protocols, e.g., when using the hexagonal electrode. The central needle is active in a total of 6 electrode pairs, so a cumulative 48 pulses are delivered. Undesirable heating and necrosis may therefore occur in the areas around the electrodes (Zmuc et al. 2019), especially at the needle tips, posing a potential risk to anatomical structures that are sensitive to thermal damage, such as bile ducts and nerves. Special care must be taken when placing the electrodes, to avoid damage to sensitive structures near the treatment zone.

## 6.2 The Basics of Patient-Specific Treatment Planning

As can be inferred from the number of factors affecting the electric field, determining the distribution of the electric field in the target tissue is not a simple task. Since the success of all EP-based treatments depends on complete coverage of the clinical target volume (CTV) with a sufficiently high electric field, it is advisable to use some form of treatment planning to ensure a successful treatment outcome (Miklavčič et al. 2010; Županič et al. 2012; Kos 2017). Treatment planning based on numerical models and computation of electric field has shown promise for guiding the physicians and veterinarians performing electroporation procedures. In 2015, Visifield ([www.visifield.com](http://www.visifield.com), University of Ljubljana, Slovenia) the first online tool for construction of patient-specific plans for EP-based treatments, was implemented (Pavliha et al. 2013; Marčan et al. 2015). However, the tool is currently intended for research and proof of concept and is not yet available for clinical use.

Patient-specific treatment planning is based on constructing an anatomically accurate numerical model from patients' medical images (MRI, CT scan). First, the patients' preinterventional images are segmented into tissues of interest, namely the tumor mass, surrounding healthy tissue, and other nearby important anatomical structures such as blood vessels and bile ducts. A 3D numerical model is then constructed from the segmented tissue masks and imported into the software for finite element analysis, such as Comsol Multiphysics ([www.comsol.com](http://www.comsol.com), Comsol Inc., Sweden) and FreeFem++ (<https://freefem.org/>, UPMC, France) (Hecht 2012). Specific electrical properties are assigned to each tissue in the model to reflect the inhomogeneity in the treated CTV. The next step is to determine the insertion trajectory and placement of the electrodes while considering any anatomical limitations. Finally, we must determine the optimal number and positions of the electrodes and the optimal parameters of applied electric pulses—mainly the amplitude of pulses and, where possible, also the number of applied pulses. Electric field distribution is then computed in the model using the finite element method. The numerical methods for the computation of electric field during electroporation are explained in more detail in Sects. 3.5 and 3.6. The finalized treatment plan provides the physician with a graphical representation of the electrode insertion trajectory and

final placement in the CTV, optimal pulse parameters to be delivered to specified electrode pairs, and a visualization of the expected electric field distribution in tissue and coverage of the CTV (Županič et al. 2012).

When creating a treatment plan, the goal is to ensure complete coverage of the CTV with minimal damage to (surrounding) critical anatomical structures, while ensuring the electrode placement and pulse delivery is technically feasible. In search of the optimal treatment parameters, several difficulties need to be overcome. First of all, we are limited by the hardware specifications of commercially available pulse generators, namely the maximum available voltage supply (3000 V) and maximum allowed electric current (50 A). Even when staying inside the boundaries of available voltage amplitude, increasing the voltage presents a risk of a high current draw in tissues with higher electrical conductivity (note: tissue conductivity also increases during electroporation). Additionally, if the CTV is too large and the electrodes are positioned too far apart it may be impossible to cover the whole CTV with a sufficiently high electric field to ensure successful treatment. The use of optimization algorithms can simplify the search for appropriate electrode positions and voltages. The limitations need to be formulated as a criterion function, which is then minimized during the optimization process, resulting in the best candidate solution for the specified problem (Županič et al. 2012; Kos 2017). Examples of criterion functions for ECT and IRE ablation are as follows:

$$F_{\text{ECT}} = -100 \cdot \text{CTV}_{\text{REV}} + 10 \cdot V_{\text{IRE}} + I_{\text{MAX}}, \quad (11)$$

$$F_{\text{IRE}} = -100 \cdot \text{CTV}_{\text{IRE}} + 10 \cdot V_{\text{IRE}} + 10 \cdot I_{\text{MAX}}, \quad (12)$$

where  $\text{CTV}_{\text{ECT}}$  and  $\text{CTV}_{\text{IRE}}$  are the volumes of CTV covered in electric field sufficient to cause reversible and irreversible electroporation respectively,  $V_{\text{IRE}}$  is the volume of surrounding healthy tissue subjected to IRE and  $I_{\text{MAX}}$  is the maximum delivered electric current. In treatment, we wish to minimize the IRE of healthy tissue and avoid a large current draw; therefore, the contributions from terms  $V_{\text{IRE}}$  and  $I_{\text{MAX}}$  increase the value of the fitness function. The optimal solution will have the lowest criterion function and the lowest contributions from “undesired” terms. Eqs. (11) and (12) are just simple examples of criterion functions—there are many ways to formulate the optimization problem.

Treatment plans are currently prepared a few days ahead of intervention using patients’ preinterventional images. Their usefulness for the physician is limited since exact electrode placement according to the plan is often difficult to achieve due to anatomical constraints and other technical difficulties. Coupling the preinterventional treatment plan with navigation systems aids in more accurate electrode placement (Grošelj et al. 2015; Fuhrmann et al. 2018). To truly utilize the potential that treatment planning offers, the whole process would need to be translated from preinterventional phase to the interventional phase—meaning, the plan being prepared during the procedure using actual electrode placement and with real-time control of the applied parameters. Nevertheless, treatment planning in its current realization provides a useful guide for the physicians and veterinarians performing EP-based treatments (Kos et al. 2010, 2015; Garcia et al. 2017; Gallinato et al. 2019).

Although treatment planning is currently mainly applied in human procedures, there are a few studies, where the possibilities of treatment planning are also demonstrated for veterinary procedures. In a case report by Kulbacka et al. (2017), a large oral melanoma in a canine patient was treated with a combination of ECT and surgery with promising results. The authors demonstrated the possibility of performing treatment planning using specialized software such as Visifield to increase the efficacy of ECT in veterinary oncology. In another prospective clinical study, seven canine patients were treated with IRE ablation for spontaneous malignant glioma using MRI-based treatment planning (Rossmeisler et al. 2015; Garcia et al. 2017). The authors prepared patient-specific numerical models to determine the pulse parameters used in the procedures and evaluated the predictive power of the treatment planning software using radiologically confirmed clinical outcomes. The results of the study show that the numerical models can evaluate the necessary treatment parameters and effectively predict clinical outcomes. The application of treatment planning in veterinary procedures could result in a more effective treatment.

---

## 7 Conclusion

Cell electroporation mainly depends on the local electric field strength and parameters of delivered pulses (pulse number, duration, and delivery rate). Fixed and variable electrode geometries can be used efficiently; however, the depth of electric field penetration and the extent of treated zone around the electrodes is very limited. Therefore, repositioning of fixed electrodes and the use of multiple electrode pairs (in case of single needle electrodes) are suggested to effectively cover the target tissue volume. Increasing the number of pulses can improve the efficacy of treatment to a limited extent; however, it also increases the risk of thermal damage to tissue, which can result in damage to critical anatomical structures (bile ducts, nerves, vessels, etc.) and a longer times to resolve the dead tissue. Numerical modelling has proven to be an indispensable tool in investigating and designing electroporation-based treatments and preparing patient-specific treatment plans. Numerical models can evaluate the necessary treatment parameters and effectively predict clinical outcomes. The application of treatment planning in veterinary procedures could result in more effective treatments.

---

## References

- Agnass P, van Veldhuisen E, van Gemert MJC et al (2020) Mathematical modeling of the thermal effects of irreversible electroporation for in vitro, in vivo, and clinical use: a systematic review. *Int J Hyperth* 37:486–505. <https://doi.org/10.1080/02656736.2020.1753828>
- Ahmed M, Brace CL, Lee FT, Goldberg SN (2011) Principles of and advances in percutaneous ablation. *Radiology* 258:351–369. <https://doi.org/10.1148/radiol.10081634>

- Arena CB, Sano MB, Rossmeisl JH et al (2011) High-frequency irreversible electroporation (H-FIRE) for non-thermal ablation without muscle contraction. *Biomed Eng Online* 10:102. <https://doi.org/10.1186/1475-925X-10-102>
- Aycock KN, Davalos RV (2019) Irreversible electroporation: background, theory, and review of recent developments in clinical oncology. *Bioelectricity* 1:214–234. <https://doi.org/10.1089/bioe.2019.0029>
- Ben-David E, Appelbaum L, Sosna J et al (2012) Characterization of irreversible electroporation ablation in in vivo porcine liver. *AJR Am J Roentgenol* 198:W62–W68. <https://doi.org/10.2214/AJR.11.6940>
- Bertacchini C (2017) Cliniporator: medical electroporation of tumors. In: Miklavcic D (ed) *Handbook of electroporation*. Springer International Publishing, Cham, pp 1–36
- Brock RM, Beitel-White N, Davalos RV, Allen IC (2020) Starting a fire without flame: the induction of cell death and inflammation in electroporation-based tumor ablation strategies. *Front Oncol* 10:1235. <https://doi.org/10.3389/fonc.2020.01235>
- Campana LG, Edhemovic I, Soden D et al (2019) Electrochemotherapy - emerging applications technical advances, new indications, combined approaches, and multi-institutional collaboration. *Eur J Surg Oncol* 45:92–102. <https://doi.org/10.1016/j.ejso.2018.11.023>
- Cannon R, Ellis S, Hayes D et al (2013) Safety and early efficacy of irreversible electroporation for hepatic tumors in proximity to vital structures. *J Surg Oncol* 107:544–549. <https://doi.org/10.1002/jso.23280>
- Čemažar M (2017) Effects of electroporation of mammalian cells on cytoskeleton and intercellular connections. In: Miklavčič D (ed) *Handbook of electroporation*. Springer International Publishing, Cham, pp 307–321
- Cemazar M, Parkins CS, Holder AL et al (2001) Electroporation of human microvascular endothelial cells: evidence for an anti-vascular mechanism of electrochemotherapy. *Br J Cancer* 84:565–570. <https://doi.org/10.1054/bjoc.2000.1625>
- Cemazar M, Tamzali Y, Sersa G et al (2008) Electrochemotherapy in veterinary oncology. *J Vet Intern Med* 22:826–831. <https://doi.org/10.1111/j.1939-1676.2008.0117.x>
- Cornelis FH, Cindrič H, Kos B et al (2020) Peri-tumoral metallic implants reduce the efficacy of irreversible electroporation for the ablation of colorectal liver metastases. *Cardiovasc Intervent Radiol* 43(1):84–93. <https://doi.org/10.1007/s00270-019-02300-y>
- Corovic S, Lackovic I, Sustaric P et al (2013) Modeling of electric field distribution in tissues during electroporation. *Biomed Eng Online* 12:16. <https://doi.org/10.1186/1475-925X-12-16>
- Davalos RV, Mir ILM, Rubinsky B (2005) Tissue ablation with irreversible electroporation. *Ann Biomed Eng* 33:223–231
- Denzi A, Strigari L, Di Filippo F et al (2015) Modeling the positioning of single needle electrodes for the treatment of breast cancer in a clinical case. *Biomed Eng Online* 14:S1. <https://doi.org/10.1186/1475-925X-14-S3-S1>
- Dermol J, Miklavčič D (2015) Mathematical models describing Chinese Hamster ovary cell death due to electroporation in vitro. *J Membr Biol* 248:865–881. <https://doi.org/10.1007/s00232-015-9825-6>
- Dermol-Černe J, Pirč E, Miklavčič D (2020) Mechanistic view of skin electroporation – models and dosimetry for successful applications: an expert review. *Expert Opin Drug Deliv* 17:689–704. <https://doi.org/10.1080/17425247.2020.1745772>
- Duck FA (2012) *Physical properties of tissue: a comprehensive reference book*. Institute of Physics and Engineering in Medicine
- Dunki-Jacobs EM, Philips P, Martin RCG (2014) Evaluation of thermal injury to liver, pancreas and kidney during irreversible electroporation in an in vivo experimental model. *Br J Surg* 101:1113–1121. <https://doi.org/10.1002/bjs.9536>
- Edd JF, Horowitz L, Davalos RV et al (2006) In vivo results of a new focal tissue ablation technique: irreversible electroporation. *IEEE Trans Biomed Eng* 53:1409–1415. <https://doi.org/10.1109/TBME.2006.873745>

- Faroja M, Ahmed M, Appelbaum L et al (2013) Irreversible electroporation ablation: is all the damage nonthermal? *Radiology* 266:462–470. <https://doi.org/10.1148/radiol.12120609>
- Fuhrmann I, Probst U, Wiggermann P, Beyer L (2018) Navigation systems for treatment planning and execution of percutaneous irreversible electroporation. *Technol Cancer Res Treat* 17:1533033818791792. <https://doi.org/10.1177/1533033818791792>
- Gabriel S, Lau RW, Gabriel C (1996) The dielectric properties of biological tissues: II. Measurements in the frequency range 10 Hz to 20 GHz. *Phys Med Biol* 41:2251–2269
- Gabriel C, Peyman A, Grant EH (2009) Electrical conductivity of tissue at frequencies below 1 MHz. *Phys Med Biol* 54:4863–4878. <https://doi.org/10.1088/0031-9155/54/16/002>
- Gallinato O, de Senneville BD, Seror O, Poignard C (2019) Numerical workflow of irreversible electroporation for deep-seated tumor. *Phys Med Biol* 64:055016. <https://doi.org/10.1088/1361-6560/ab00c4>
- Garcia PA, Rossmesl JH, Neal RE et al (2011) A parametric study delineating irreversible electroporation from thermal damage based on a minimally invasive intracranial procedure. *Biomed Eng Online* 10:34. <https://doi.org/10.1186/1475-925X-10-34>
- Garcia PA, Davalos RV, Miklavcic D (2014) A numerical investigation of the electric and thermal cell kill distributions in electroporation-based therapies in tissue. *PLoS One* 9:e103083. <https://doi.org/10.1371/journal.pone.0103083>
- Garcia PA, Kos B, Rossmesl JH et al (2017) Predictive therapeutic planning for irreversible electroporation treatment of spontaneous malignant glioma. *Med Phys* 44:4968–4980. <https://doi.org/10.1002/mp.12401>
- García-Sánchez T, Leray I, Ronchetti M et al (2019) Impact of the number of electric pulses on cell electrochemotherapy in vitro: limits of linearity and saturation. *Bioelectrochemistry* 129:218–227. <https://doi.org/10.1016/j.bioelechem.2019.05.021>
- Geboers B, Scheffer HJ, Graybill PM et al (2020) High-voltage electrical pulses in oncology: irreversible electroporation, electrochemotherapy, gene electrotransfer, electrofusion, and electroimmunotherapy. *Radiology* 295:254–272. <https://doi.org/10.1148/radiol.2020192190>
- Gehl J, Sersa G, Matthiessen LW et al (2018) Updated standard operating procedures for electrochemotherapy of cutaneous tumours and skin metastases. *Acta Oncol* 57:874–882. <https://doi.org/10.1080/0284186X.2018.1454602>
- Golberg A, Rubinsky B (2010) A statistical model for multidimensional irreversible electroporation cell death in tissue. *BioMed Eng Online* 9:13. <https://doi.org/10.1186/1475-925X-9-13>
- Golberg A, Rubinsky B (2012) Towards electroporation based treatment planning considering electric field induced muscle contractions. *Technol Cancer Res Treat* 11:189–201. <https://doi.org/10.7785/tcrt.2012.500249>
- Gothelf A, Gehl J (2010) Gene electrotransfer to skin; review of existing literature and clinical perspectives. *Curr Gene Ther* 10:287–299. <https://doi.org/10.2174/156652310791823443>
- Graybill PM, Davalos RV (2020) Cytoskeletal disruption after electroporation and its significance to pulsed electric field therapies. *Cancers (Basel)* 12:1132. <https://doi.org/10.3390/cancers12051132>
- Grošelj A, Kos B, Čemažar M et al (2015) Coupling treatment planning with navigation system: a new technological approach in treatment of head and neck tumors by electrochemotherapy. *Biomed Eng Online* 14(Suppl 3):S2. <https://doi.org/10.1186/1475-925X-14-S3-S2>
- Haemmerich D, Schutt DJ, Wright AW et al (2009) Electrical conductivity measurement of excised human metastatic liver tumours before and after thermal ablation. *Physiol Meas* 30:459–466. <https://doi.org/10.1088/0967-3334/30/5/003>
- Hecht F (2012) New development in freefem++. *J Numer Math* 20:251–266. <https://doi.org/10.1515/jnum-2012-0013>
- Heller R, Heller LC (2015) Chapter eight-gene electrotransfer clinical trials. In: Huang L, Liu D, Wagner E (eds) *Advances in genetics*. Academic, pp 235–262
- Hjouj M, Last D, Guez D et al (2012) MRI study on reversible and irreversible electroporation induced blood brain barrier disruption. *PLoS One* 7:e42817. <https://doi.org/10.1371/journal.pone.0042817>

- Ivorra A, Al-Sakere B, Rubinsky B, Mir LM (2009) In vivo electrical conductivity measurements during and after tumor electroporation: conductivity changes reflect the treatment outcome. *Phys Med Biol* 54:5949. <https://doi.org/10.1088/0031-9155/54/19/019>
- Jarm T, Cemazar M, Miklavcic D, Sersa G (2010) Antivascular effects of electrochemotherapy: implications in treatment of bleeding metastases. *Expert Rev Anticancer Ther* 10:729–746. <https://doi.org/10.1586/era.10.43>
- Jiang C, Davalos RV, Bischof JC (2015) A review of basic to clinical studies of irreversible electroporation therapy. *IEEE Trans Biomed Eng* 62:4–20. <https://doi.org/10.1109/TBME.2014.2367543>
- Kanthou C, Kranjc S, Sersa G et al (2006) The endothelial cytoskeleton as a target of electroporation-based therapies. *Mol Cancer Ther* 5:3145–3152. <https://doi.org/10.1158/1535-7163.MCT-06-0410>
- Kos B (2017) Treatment planning for electrochemotherapy and irreversible electroporation of deep-seated tumors. In: Miklavčič D (ed) *Handbook of electroporation*. Springer International Publishing, Cham, pp 1001–1017
- Kos B, Županič A, Kotnik T et al (2010) Robustness of treatment planning for electrochemotherapy of deep-seated tumors. *J Membr Biol* 236:147–153. <https://doi.org/10.1007/s00232-010-9274-1>
- Kos B, Voigt P, Miklavcic D, Moche M (2015) Careful treatment planning enables safe ablation of liver tumors adjacent to major blood vessels by percutaneous irreversible electroporation (IRE). *Radiol Oncol* 49:234–241. <https://doi.org/10.1515/raon-2015-0031>
- Kotnik T, Pucihar G, Miklavčič D (2011) The cell in the electric field. In: *Clinical aspects of electroporation*. Springer, New York, NY, pp 19–29
- Kotnik T, Frey W, Sack M et al (2015) Electroporation-based applications in biotechnology. *Trends Biotechnol* 33:480–488. <https://doi.org/10.1016/j.tibtech.2015.06.002>
- Kotnik T, Rems L, Tarek M, Miklavčič D (2019) Membrane electroporation and electropermeabilization: mechanisms and models. *Annu Rev Biophys* 48:63–91. <https://doi.org/10.1146/annurev-biophys-052118-115451>
- Kulbacka J, Paczuska J, Rembiałkowska N et al (2017) Electrochemotherapy combined with standard and CO<sub>2</sub> laser surgeries in canine oral melanoma. *Slov Vet Res* 54:181–186. <https://doi.org/10.26873/SVR-322-2017>
- Lacković I, Magjarević R, Miklavčič D (2009) Three-dimensional finite-element analysis of joule heating in electrochemotherapy and in vivo gene electrotransfer. *IEEE Trans Dielectr Electr Insul* 16:1338–1347. <https://doi.org/10.1109/TDEI.2009.5293947>
- Lambrecht L, Lopes A, Kos S et al (2016) Clinical potential of electroporation for gene therapy and DNA vaccine delivery. *Expert Opin Drug Deliv* 13:295–310. <https://doi.org/10.1517/17425247.2016.1121990>
- Lamprecht U, Tratariu U, Loiacono L, Cemazar M et al (2017) Gene electrotransfer of plasmid-encoding IL-12 recruits the M1 macrophages and antigen-presenting cells inducing the eradication of aggressive B16F10 murine melanoma. *Mediat Inflamm* 2017:e5285890. <https://doi.org/10.1155/2017/5285890>
- Laufer S, Ivorra A, Reuter VE et al (2010) Electrical impedance characterization of normal and cancerous human hepatic tissue. *Physiol Meas* 31:995–1009. <https://doi.org/10.1088/0967-3334/31/7/009>
- Maglietti F, Michinski S, Olainz N et al (2013) The role of Ph fronts in tissue electroporation based treatments. *PLoS One* 8:e80167. <https://doi.org/10.1371/journal.pone.0080167>
- Mahnič-Kalamiza S, Vorobiev E, Miklavčič D (2014) Electroporation in food processing and biorefinery. *J Membr Biol* 247:1279–1304. <https://doi.org/10.1007/s00232-014-9737-x>
- Mali B, Gorjup V, Edhemovic I et al (2015) Electrochemotherapy of colorectal liver metastases - an observational study of its effects on the electrocardiogram. *Biomed Eng Online* 14:S5. <https://doi.org/10.1186/1475-925X-14-S3-S5>
- Maor E, Ivorra A, Mitchell JJ, Rubinsky B (2010) Vascular smooth muscle cells ablation with endovascular nonthermal irreversible electroporation. *J Vasc Interv Radiol* 21:1708–1715. <https://doi.org/10.1016/j.jvir.2010.06.024>

- Marčan M, Pavliha D, Kos B et al (2015) Web-based tool for visualization of electric field distribution in deep-seated body structures and planning of electroporation-based treatments. *Biomed Eng Online* 14(Suppl 3):S4. <https://doi.org/10.1186/1475-925X-14-S3-S4>
- Martin RC, Schwartz E, Adams J et al (2015) Intra - operative anesthesia management in patients undergoing surgical irreversible electroporation of the pancreas, liver, kidney, and retroperitoneal tumors. *Anesth Pain Med* 5:e22786. <https://doi.org/10.5812/aapm.22786>
- Meijerink MR, Scheffer HJ, Narayanan G (eds) (2018) Irreversible electroporation in clinical practice. Springer International Publishing
- Mercadal B, Arena CB, Davalos RV, Ivorra A (2017) Avoiding nerve stimulation in irreversible electroporation: a numerical modeling study. *Phys Med Biol* 62:8060–8079. <https://doi.org/10.1088/1361-6560/aa8c53>
- Miklavčič D, Serša G, Kryžanowski M et al (1993) Tumor treatment by direct electric current-tumor temperature and pH, electrode material and configuration. *Bioelectrochem Bioenerg* 30:209–220. [https://doi.org/10.1016/0302-4598\(93\)80080-E](https://doi.org/10.1016/0302-4598(93)80080-E)
- Miklavčič D, Pucihar G, Pavlovac M et al (2005) The effect of high frequency electric pulses on muscle contractions and antitumor efficiency in vivo for a potential use in clinical electrochemotherapy. *Bioelectrochemistry* 65:121–128. <https://doi.org/10.1016/j.bioelechem.2004.07.004>
- Miklavčič D, Čorović S, Pucihar G, Pavšelj N (2006) Importance of tumour coverage by sufficiently high local electric field for effective electrochemotherapy. *Eur J Cancer Suppl* 4:45–51. <https://doi.org/10.1016/j.ejcsup.2006.08.006>
- Miklavčič D, Snoj M, Županič A et al (2010) Towards treatment planning and treatment of deep-seated solid tumors by electrochemotherapy. *Biomed Eng Online* 9:10. <https://doi.org/10.1186/1475-925X-9-10>
- Miklavčič D, Serša G, Breclj E et al (2012) Electrochemotherapy: technological advancements for efficient electroporation-based treatment of internal tumors. *Med Biol Eng Comput* 50:1213–1225. <https://doi.org/10.1007/s11517-012-0991-8>
- Miklavčič D, Mali B, Kos B et al (2014) Electrochemotherapy: from the drawing board into medical practice. *Biomed Eng Online* 13:29. <https://doi.org/10.1186/1475-925X-13-29>
- Mir LM, Orlowski S, Belehradek J, Paoletti C (1991) Electrochemotherapy potentiation of antitumour effect of bleomycin by local electric pulses. *Eur J Cancer* 27:68–72
- Mir LM, Gehl J, Sersa G et al (2006) Standard operating procedures of the electrochemotherapy: instructions for the use of bleomycin or cisplatin administered either systemically or locally and electric pulses delivered by the Cliniporator TM by means of invasive or non-invasive electrodes. *Eur J Cancer Suppl* 4:14–25. <https://doi.org/10.1016/j.ejcsup.2006.08.003>
- Neumann E, Rosenheck K (1972) Permeability changes induced by electric impulses in vesicular membranes. *J Membr Biol* 10:279–290. <https://doi.org/10.1007/BF01867861>
- O'Brien TJ, Bonakdar M, Bhonsle S et al (2018) Effects of internal electrode cooling on irreversible electroporation using a perfused organ model. *Int J Hyperthermia* 35(1):44–55. <https://doi.org/10.1080/02656736.2018.1473893>
- O'Rourke AP, Lazebnik M, Bertram JM et al (2007) Dielectric properties of human normal, malignant and cirrhotic liver tissue: in vivo and ex vivo measurements from 0.5 to 20 GHz using a precision open-ended coaxial probe. *Phys Med Biol* 52:4707–4719. <https://doi.org/10.1088/0031-9155/52/15/022>
- Obermeier B, Daneman R, Ransohoff RM (2013) Development, maintenance and disruption of the blood-brain barrier. *Nat Med* 19:1584–1596. <https://doi.org/10.1038/nm.3407>
- Olaiz N, Signori E, Maglietti F et al (2014) Tissue damage modeling in gene electrotransfer: the role of pH. *Bioelectrochemistry* 100:105–111. <https://doi.org/10.1016/j.bioelechem.2014.05.001>
- Pavliha D, Kos B, Marčan M et al (2013) Planning of electroporation-based treatments using Web-based treatment-planning software. *J Membr Biol* 246:833–842. <https://doi.org/10.1007/s00232-013-9567-2>
- Pavšelj N, Miklavčič D (2008) Numerical modeling in electroporation-based biomedical applications. *Radiol Oncol* 42:93–101

- Pavšelj N, Bregar Z, Cukjati D et al (2005) The course of tissue permeabilization studied on a mathematical model of a subcutaneous tumor in small animals. *IEEE Trans Biomed Eng* 52:1373–1381. <https://doi.org/10.1109/TBME.2005.851524>
- Peleg M (1995) A model of microbial survival after exposure to pulsed electric fields. *J Sci Food Agric* 67:93–99. <https://doi.org/10.1002/jsfa.2740670115>
- Pennes HH (1948) Analysis of tissue and arterial blood temperatures in the resting human forearm. *J Appl Physiol* 85:93–122. <https://doi.org/10.1152/jappl.1948.1.2.93>
- Peyman A, Kos B, Djokić M et al (2015) Variation in dielectric properties due to pathological changes in human liver. *Bioelectromagnetics* 36:603–612. <https://doi.org/10.1002/bem.21939>
- Potočnik T, Miklavčič D, Maček Lebar A (2019) Effect of electroporation and recovery medium pH on cell membrane permeabilization, cell survival and gene transfer efficiency in vitro. *Bioelectrochemistry* 130:107342. <https://doi.org/10.1016/j.bioelechem.2019.107342>
- Pucihar G, Krmelj J, Reberšek M et al (2011) Equivalent pulse parameters for electroporation. *IEEE Trans Biomed Eng* 58:3279–3288. <https://doi.org/10.1109/TBME.2011.2167232>
- Reddy VY, Koruth J, Jais P et al (2018) Ablation of atrial fibrillation with pulsed electric fields: an ultra-rapid, tissue-selective modality for cardiac ablation. *J Am Coll Cardiol EP* 4:987–995. <https://doi.org/10.1016/j.jacep.2018.04.005>
- Rems L, Miklavčič D (2016) Tutorial: electroporation of cells in complex materials and tissue. *J Appl Phys* 119:201101. <https://doi.org/10.1063/1.4949264>
- Ringel-Scaia VM, Beitel-White N, Lorenzo MF et al (2019) High-frequency irreversible electroporation is an effective tumor ablation strategy that induces immunologic cell death and promotes systemic anti-tumor immunity. *EBioMedicine* 44:112–125. <https://doi.org/10.1016/j.ebiom.2019.05.036>
- Rosazza C, Meglic SH, Zumbusch A et al (2016) Gene electrotransfer: a mechanistic perspective. *Curr Gene Ther* 16:98–129
- Rossmanna C, Haemmerich D (2014) Review of temperature dependence of thermal properties, dielectric properties, and perfusion of biological tissues at hyperthermic and ablation temperatures. *Crit Rev Biomed Eng* 42:467–492
- Rossmesl JH, Garcia PA, Pancotto TE et al (2015) Safety and feasibility of the NanoKnife system for irreversible electroporation ablative treatment of canine spontaneous intracranial gliomas. *J Neurosurg* 123:1008–1025. <https://doi.org/10.3171/2014.12.JNS141768>
- Rubinsky B (2007) Irreversible electroporation in medicine. *Technol Cancer Res Treat* 6:255–259. <https://doi.org/10.1177/153303460700600401>
- Sano MB, Petrella RA, Kaufman JD et al (2020) Electro-thermal therapy: microsecond duration pulsed electric field tissue ablation with dynamic temperature control algorithms. *Comput Biol Med* 121:103807. <https://doi.org/10.1016/j.compbiomed.2020.103807>
- Scheffer HJ, Nielsen K, de Jong MC et al (2014) Irreversible electroporation for nonthermal tumor ablation in the clinical setting: a systematic review of safety and efficacy. *J Vasc Interv Radiol* 25:997–1011.; quiz 1011. <https://doi.org/10.1016/j.jvir.2014.01.028>
- Schoellnast H, Monette S, Ezell PC et al (2013) The delayed effects of irreversible electroporation ablation on nerves. *Eur Radiol* 23:375–380. <https://doi.org/10.1007/s00330-012-2610-3>
- Schutt DJ, Haemmerich D (2008) Effects of variation in perfusion rates and of perfusion models in computational models of radio frequency tumor ablation. *Med Phys* 35:3462–3470. <https://doi.org/10.1118/1.2948388>
- Šel D, Cukjati D, Batiškaite D et al (2005) Sequential finite element model of tissue electroporeabilization. *IEEE Trans Biomed Eng* 52:816–827. <https://doi.org/10.1109/TBME.2005.845212>
- Šel D, Maček Lebar A, Miklavčič D (2007) Feasibility of employing model-based optimization of pulse amplitude and electrode distance for effective tumor electroporeabilization. *IEEE Trans Biomed Eng* 54:773–781. <https://doi.org/10.1109/TBME.2006.889196>
- Serša G, Miklavčič D (2008) Electrochemotherapy of tumours. *J Vis Exp* 22:1038. <https://doi.org/10.3791/1038>

- Serša G, Čemažar M, Šemrov D, Miklavčič D (1996) Changing electrode orientation improves the efficacy of electrochemotherapy of solid tumors in mice. *Bioelectrochem Bioenerg* 39:61–66. [https://doi.org/10.1016/0302-4598\(95\)01866-2](https://doi.org/10.1016/0302-4598(95)01866-2)
- Sharabi S, Mardor Y (2016) Effect of electroporation on blood-brain barrier. In: Miklavcic D (ed) Handbook of electroporation. Springer International Publishing, Cham, pp 1–17
- Sharabi S, Kos B, Last D et al (2016) A statistical model describing combined irreversible electroporation and electroporation-induced blood-brain barrier disruption. *Radiol Oncol* 50:28–38. <https://doi.org/10.1515/raon-2016-0009>
- Sharabi S, Bresler Y, Ravid O et al (2019) Transient blood–brain barrier disruption is induced by low pulsed electrical fields in vitro: an analysis of permeability and trans-endothelial electric resistivity. *Drug Deliv* 26:459–469. <https://doi.org/10.1080/10717544.2019.1571123>
- Stepišnik T, Jarm T, Grošelj A et al (2016) Electrochemotherapy – an effective method for treatment of tumors with combination of chemotherapeutic agent and electric field. *Slov Med J* 85
- Stewart MT, Haines DE, Verma A et al (2019) Intracardiac pulsed field ablation: proof of feasibility in a chronic porcine model. *Heart Rhythm* 16:754–764. <https://doi.org/10.1016/j.hrthm.2018.10.030>
- Turjanski P, Olaiz N, Abou-Adal P et al (2009) pH front tracking in the electrochemical treatment (EChT) of tumors: experiments and simulations. *Electrochim Acta* 54:6199–6206. <https://doi.org/10.1016/j.electacta.2009.05.062>
- Turjanski P, Olaiz N, Maglietti F et al (2011) The Role of pH Fronts in Reversible Electroporation. *PLoS One* 6:e17303. <https://doi.org/10.1371/journal.pone.0017303>
- Vogel JA, van Veldhuisen E, Agnass P et al (2016) Time-dependent impact of irreversible electroporation on pancreas, liver, blood vessels and nerves: a systematic review of experimental studies. *PLoS One* 11:e0166987. <https://doi.org/10.1371/journal.pone.0166987>
- Wagstaff PGK, de Bruin DM, van den Bos W et al (2015) Irreversible electroporation of the porcine kidney: temperature development and distribution. *Urol Oncol* 33:168.e1–168.e7. <https://doi.org/10.1016/j.urolonc.2014.11.019>
- Wittkampf FHM, van Es R, Neven K (2018) Electroporation and its relevance for cardiac catheter ablation. *JACC Clin Electrophysiol* 4:977–986. <https://doi.org/10.1016/j.jacep.2018.06.005>
- Yao C, Dong S, Zhao Y et al (2017) Bipolar microsecond pulses and insulated needle electrodes for reducing muscle contractions during irreversible electroporation. *IEEE Trans Biomed Eng* 64:2924–2937. <https://doi.org/10.1109/TBME.2017.2690624>
- Yarmush ML, Golberg A, Serša G et al (2014) Electroporation-based technologies for medicine: principles, applications, and challenges. *Annu Rev Biomed Eng* 16:295–320. <https://doi.org/10.1146/annurev-bioeng-071813-104622>
- Zhao Y, Zheng S, Beitel-White N et al (2020) Development of a multi-pulse conductivity model for liver tissue treated with pulsed electric fields. *Front Bioeng Biotechnol* 8:396. <https://doi.org/10.3389/fbioe.2020.00396>
- Zmuc J, Gasljevic G, Sersa G et al (2019) Large liver blood vessels and bile ducts are not damaged by electrochemotherapy with bleomycin in pigs. *Sci Rep* 9:3649. <https://doi.org/10.1038/s41598-019-40395-y>
- Zupanic A, Ribaric S, Miklavcic D (2007) Increasing the repetition frequency of electric pulse delivery reduces unpleasant sensations that occur in electrochemotherapy. *Neoplasma* 54:246–250
- Županič A, Kos B, Miklavčič D (2012) Treatment planning of electroporation-based medical interventions: electrochemotherapy, gene electrotransfer and irreversible electroporation. *Phys Med Biol* 57:5425–5440. <https://doi.org/10.1088/0031-9155/57/17/5425>